SLAC-PUB-2615
September 1980
(T/E)

e^+e^- PHYSICS TODAY AND TOMORROW:

Four Tutorial Lectures Delivered at the

Arctic School of Physics 1980*

Martin L. Perl

Stanford Linear Accelerator Center
Stanford University, Stanford, California 94305

(Arctic School of Physics, Akaslompolo, Finland, Sponsored by University of Helsinki, July 27 - August 7, 1980.)

*Work supported by the Department of Energy, Contract DE-AC03-76SF00515.

Lecture 1: BASIC CONCEPTS

These four tutorial lectures were delivered at the Arctic School of Physics in August, 1980. The purpose of these lectures was to provide an introduction to high energy positron-electron annihilation physics; and to serve as a foundation for the more advanced lectures at the school. I have tried to accomplish this task by discussing selected topics, rather than by surveying the field.

In this first lecture I discuss three subjects: the parameters of e^+e^- storage rings which are directly relevant to experiments; the physics of e^+e^- one-photon-exchange as illustrated by the reaction $e^+e^- \to \mu^+\mu^-$; and the naive quark model for the reaction $e^+e^- \to$ hadrons.

The second lecture is devoted to heavy leptons: the status of the tau lepton; and the status of the search for heavier leptons.

In the third lecture I discuss the non-relativistic quantum mechanics of heavy quark-antiquark systems — the ψ/J particle family and the Υ particle family. I leave to other lecturers topics related to single charm and single bottom hadrons. And I also leave to others the discussion of the extensive work which has been done in the past two years on the dynamics of quarks and gluons in hadron jets.

The fourth lecture concerns the "tomorrow" in the title of these lectures. As e^+e^- colliding beams machines attain very high energy, $E_{c.m.} \gtrsim 50$ GeV, e^+e^- annihilation will occur through the weak interactions as well as through the electromagnetic interaction. This will allow the study of the weak interactions and the study of any new particles related to, or produced through, the weak interactions. Lecture 4 discusses this physics at an energy corresponding to the mass of the Z° intermediate

boson, assuming the Z^0 exists; and then discusses the physics at yet higher energy. The lecture concludes with a description of the capabilities and limitations of the e^+e^- colliding beams machines needed to attain this very high energy--both storage rings and colliding linear accelerators.

I have provided each lecture with a short set of references whose purpose is tutorial. This is not a review, and I hope I will be excused for sometimes omitting references to original or recent works.

1A: e^+e^- Storage Rings

Basic Design: In a positron-electron colliding beams storage ring[1.1,1.2] e^+ and e^- bunches travel in opposite directions, Fig. 1.1a; and the bunches collide in the interaction regions. The e^+ and e^- bunches may travel in the same ring, Fig. 1.1a; or they may travel in separate rings, Fig. 1.1b, which intersect at the interaction regions. Consider the simplest case of a single ring of circumference C, one bunch each of e^+ and e^-, with each bunch containing N particles. There are two interaction regions. A reaction $e^+ + e^- \to X$ with cross section σ will yield per interaction region

$$\mathcal{N}(\text{events/sec}) = \sigma\mathscr{L} \tag{1.1}$$

$\mathscr{L}$ is called the luminosity; its units are $\text{cm}^{-2}\ \text{sec}^{-1}$ when σ is in cm^2.

The luminosity is one of the two basic properties of a storage ring; the other is the energy of each e^+ or e^-, often called the beam energy, E. In the usual design in which the e^+ and e^- collide head-on, the total momentum of the e^+e^- system is zero; and the total energy is

$$E_{c.m.} = 2E \tag{1.2}$$

Here the subscript c.m. means center of mass, since the laboratory frame is also the center of mass frame. We often use $s = E^2_{c.m.}$.

Luminosity: Returning to $\mathscr{L}$, the e^+ or e^- bunches are of the order of millimeters to centimeters in length while the circumferences of rings are hundreds to thousands of meters long. Hence the bunch length can be ignored and

$$\mathscr{L} = fN^2/A \tag{1.3}$$

where f is the frequency (Hz) with which a bunch goes around the ring, and A is the effective cross sectional area of a bunch, Fig. 1.1c. Note that $f = c/C$ where c is the velocity of light. Eq. (1.3) is for one bunch each of e^+ and e^-. For n_b bunches each of e^+ and e^-

$$\mathscr{L} = n_b fN^2/A$$

The transverse particle distribution in a bunch is not uniform; for a gaussian particle distribution with parameters σ_x, σ_y (Fig. 1.1c)

$$\mathscr{L} = n_b fN^2/(4\pi\sigma_x\sigma_y) \tag{1.4}$$

The question now arises as to how large $\mathscr{L}$ must be to give a useful event rate $\mathscr{N} = \sigma\mathscr{L}$. As I will show later in this lecture, Eqs. (1.11) and (1.20), the order of magnitude of σ is

$$\sigma \sim 10^{-31}\ \text{cm}^2/E_{\text{c.m.}}^2 \tag{1.5}$$

where $E_{\text{c.m.}}$ is in GeV. A desirable event rate of one event per minute requires

$$\mathscr{L} \sim 10^{31}\ E_{\text{c.m.}}^2/60 \sim 10^{29}\ E_{\text{c.m.}}^2\ \text{cm}^{-2}\ \text{sec}^{-1}$$

Thus at medium energy e^+e^- rings such as SPEAR and DORIS with $E_{\text{c.m.}} \sim 4$ GeV, $\mathscr{L} \sim 2 \times 10^{30}\ \text{cm}^{-2}\ \text{sec}^{-1}$ is sufficient. At high energy rings, PETRA and PEP, $E_{\text{c.m.}} \sim 30$ GeV and $\mathscr{L} \sim 10^{32}\ \text{cm}^{-2}\ \text{sec}^{-1}$ is desirable.

Hence $\mathscr{L} = 10^{32}$ cm^{-2} sec^{-1} has become the design goal of high energy e^+e^- storage rings. It would be nice to obtain even higher luminosities; however at present we don't know how to design e^+e^- rings with substantially higher luminosities.

Example: To illustrate Eq. (1.4), consider the maximum design luminosity of the PEP e^+e^- storage ring at SLAC. The parameters at $E_{c.m.} = 30$ GeV are

$$\begin{aligned} C &= 2200 \text{ m} \\ f &= 1.36 \times 10^5 \text{ Hz} \\ N &= 8.3 \times 10^{11} \\ n_b &= 3 \\ \sigma_x &= 750 \ \mu\text{m} = 0.075 \text{ cm} \\ \sigma_y &= 30 \ \mu\text{m} = 0.003 \text{ cm} \end{aligned} \tag{1.6}$$

Therefore

$$\mathscr{L} = 1.0 \times 10^{32} \text{ cm}^{-2} \text{ sec}^{-1} \tag{1.7}$$

Variation of $\mathscr{L}$ with $E_{c.m.}$: Figure 1.2 shows how the maximum luminosity of a ring typically varies with energy. There is one value of $E_{c.m.}$ with maximum luminosity, $E_{c.m.,standard}$. The ring design usually gives

$$\mathscr{L}_{max}(E_{c.m.}) = \mathscr{L}_{max}(E_{c.m.,standard})(E_{c.m.}/E_{c.m.,standard})^2 \tag{1.8}$$

when $E_{c.m.} < E_{c.m.,standard}$. At higher energy, $\mathscr{L}$ decreases quickly as the maximum $E_{c.m.}$ is approached.

Parameters of Medium and High Energy e^+e^- Storage Rings: Table 1.1 lists the parameters of presently operating and proposed medium energy and high energy e^+e^- storage rings. Very high energy rings, defined as those which can attain $E_{c.m.} \geq 90$ GeV and so produce the proposed Z^o intermediate boson, are discussed in Lecture 4, and are not listed here.

Table 1.1. Some properties of medium energy and high energy e^+e^- storage rings.

Name	Location	Status	Ec.m. range (GeV) (design)	Maximum luminosity cm^{-2} sec^{-1}
VEPP-2M	Novosibirsk	operating	0.4 - 1.4	10^{30} achieved
ALA	Frascati	proposed	1.0 - 2.4	10^{31}, design
DCI	Orsay	operating	1.0 - 3.8	10^{30}, achieved with two beams
SPEAR	Stanford	operating	2.5 - 9	$\sim 10^{31}$, achieved
DORIS	Hamburg	operating	2.0 - 10.2	$\sim 10^{31}$, achieved
VEPP-4	Novosibirsk	operating	2.0 - 14.0	10^{32}, design
CESR	Cornell	operating	6.0 - 16.0	10^{32}, design
PETRA	Hamburg	operating	10.0 - 46.0	10^{32}, design
PEP	Stanford	operating	10.0 - 46.0	10^{32}, design
HERA	Hamburg	proposed first stage of e-p machine	20.0 - 70.0	10^{32}, design

Some of the properties listed in Table 1.1 are design parameters and have not yet been achieved. At present the highest energy achieved is $E_{c.m.} \approx 37$ GeV at PETRA, and the highest achieved luminosities are 10^{31} cm^{-2} sec^{-1}. These are the experimental boundaries to our present knowledge of e^+e^- physics and to the material presented in the first three lectures.

1B: One-Photon-Exchange and the Reaction $e^+e^- \to \mu^+ + \mu^-$

The Reaction $e^+ + e^- \to \mu^+ + \mu^-$: The simple reaction[1,3]

$$e^+ + e^- \to \mu^+ + \mu^- \tag{1.8}$$

which occurs through the one-photon-exchange diagram, Fig. 1.3a, plays a basic role in e^+e^- annihilation physics. The total cross section is

$$\sigma(e^+e^- \to \mu^+\mu^-) = \frac{\pi\alpha^2(\hbar c)^2}{3E^2}\left[\frac{\beta(3-\beta^2)}{2}\right] \tag{1.9a}$$

Here E is the e^+ or e^- energy; α is the fine structure constant and equals about 1/137; β is the μ velocity divided by the velocity of light c; and $\hbar$ is Plank's constant. One usually sees Eq. (1.9) expressed in elementary particle units ($\hbar = 1$, $c = 1$)

$$\sigma(e^+e^- \to \mu^+\mu^-) = \frac{\pi\alpha^2}{3E^2}\left[\frac{\beta(3-\beta^2)}{2}\right] \tag{1.9b}$$

Equations (1.9) are very general, holding for pair production of any charged, spin 1/2, point particle except the electron. For example Eqs. (1.9) are also true for $e^+ + e^- \to \tau^+ + \tau^-$ where τ is the tau heavy lepton discussed in the next lecture. Furthermore if the produced particles have a charge q' different from the unit electric charge q,

Eqs. (1.9) are simply multiplied by $(q'/q)^2$. Equations (1.9) do not apply to the reaction $e^+ + e^- \to e^+ + e^-$ because there is an additional diagram, Fig. 1.3d.

When E is much larger than the μ mass, $\beta = 1$, and Eqs. (1.9) reduce to

$$\sigma(e^+e^- \to \mu^+\mu^-) = \frac{\pi\alpha^2}{3E^2} = \frac{4\pi\alpha^2}{3s} \tag{1.10}$$

where $s = E^2_{c.m.} = 4E^2$. And using Eq. (1.9a) and $\hbar c = 1.97 \times 10^{-14}$ GeV cm, Eq. (1.10) becomes

$$\sigma(e^+e^- \to \mu^+\mu^-) = \frac{2.17 \times 10^{-32}\ \text{cm}^2}{E^2} = \frac{21.7\ \text{nb}}{E^2} \tag{1.11}$$

where E is in GeV.

Tests of Quantum Electrodynamics: The reactions $e^+ + e^- \to \mu^+ + \mu^-$ and $e^+ + e^- \to e^+ + e^-$ allow high energy tests of the validity of the theory of quantum electrodynamics (QED). It is conventional[1.3,1.4] to consider two kinds of modifications of this theory, Fig. 1.3b: the photon propagator may be modified

$$\frac{1}{s} \to \frac{1}{s} \mp \frac{1}{s - \Lambda_\pm^2} \quad ; \tag{1.12a}$$

or the muon may be given a form factor

$$F_\mu^{(s)} = \frac{1}{1 + s/\Lambda_\mu^2} \tag{1.12b}$$

This leads to modified cross sections

$$\sigma_{mod}(e^+e^- \to \mu^+\mu^-) = \sigma_{QED}(e^+e^- \to \mu^+\mu^-)\left[1 \mp \frac{1}{1 - \Lambda_\pm^2/s}\right]^2 \tag{1.13a}$$

or

$$\sigma_{mod}(e^+e^- \to \mu^+\mu^-) = \sigma_{QED}(e^+e^- \to \mu^+\mu^-)\left[\frac{1}{1 + s/\Lambda_\mu^2}\right]^2 \qquad (1.13b)$$

where σ_{QED} is defined by Eqs. (1.9). The Λ^2 are called QED breakdown parameters. All recent experiments[1,4] show no deviation from QED; hence they find lower limits on the Λ's. Since these Λ's are larger than the $\sqrt{s}$ values of the experiments, we can make linear approximations in s to Eqs. (1.13).

$$\sigma_{mod}(e^+e^- \to \mu^+\mu^-) = \sigma_{QED}[1 \pm 2s/\Lambda_\mp^2]; \text{ propagator modified} \qquad (1.14a)$$

$$\sigma_{mod}(e^+e^- \to \mu^+\mu^-) = \sigma_{QED}[1 + 2s/\Lambda_\mu^2]; \text{ muon form factor} \qquad (1.14b)$$

Figure 1.3c shows one interpretation of a propagator modification, namely an additional diagram where a particle X of mass M and coupling constant g is exchanged. Defining r = g/e, the linear form is

$$\sigma_{mod}(e^+e^- \to \mu^+\mu^-) = \sigma_{QED}[1 + 2s/(M^2/r^2) \qquad (1.14c)$$

Indeed this will be the effect of the weak interactions[1,5] via the exchange of a Z^o.

At the PETRA e^+e^- storage ring, high energy measurements have been made of the reaction

$$e^+ + e^- \to \mu^+ + \mu^- \quad ; \qquad (1.15a)$$

as well as the other purely electromagnetic reactions

$$e^+ + e^- \to e^+ + e^- \qquad (1.15b)$$

$$e^+ + e^- \to \tau^+ + \tau^- \qquad (1.15c)$$

$$e^+ + e^- \to \gamma + \gamma \qquad (1.15d)$$

No deviations from QED have been found[1,4] and the 95% confidence lower limits on the Λ's are:

$$\Lambda \text{ lower limits} = 50 \text{ to } 200 \text{ GeV} \qquad (1.16)$$

To interpret this take Λ = 100 GeV and the $e^+e^- \to \mu^+\mu^-$ reaction. Using the linear forms, Eqs. (1.14a) and (1.14b); and taking $\sqrt{s} \sim 30$ GeV

$$\sigma_{mod}/\sigma_{QED} \approx 1.0 \pm 0.2;\ 95\%\ \text{C.L.} \tag{1.17a}$$

The form factor interpretation, Eq. (1.12b), yields

$$F_\mu(\sqrt{s} = 30\ \text{GeV}) \approx 1.0 \pm 0.1;\ 95\%\ \text{C.L.} \tag{1.17b}$$

That is, the μ is a point particle within ± 0.1 with 95% C.L. at 30 GeV. Or using the additional diagram interpretation, Fig. 1.13c and Eq. (1.14c),

$$M/r = 100\ \text{GeV} \tag{1.17c}$$

Hence if g = e in Fig. 1.13c, then M would have to be larger than 100 GeV with 95% C.L. But if $r \ll 1$, M could be $\ll$ 100 GeV.

1C: The Naive Quark Model for $e^+ + e^- \to$ hadrons

Basic Model: Non-resonant Production: The naive quark model, Fig. 1.4a for non-resonant hadron production

$$e^+ + e^- \to \text{hadrons} \tag{1.18}$$

is based upon two assumptions:

(a) The virtual photon creates a quark-antiquark pair through a purely electromagnetic interaction; the strong force, final-state interaction between the quarks being ignored. Hence this is simply the reaction discussed in Section 1B with non-unit charges.

(b) All quark-antiquark pairs materialize as hadrons; there are no free quarks.

Quantitatively

$$\sigma(e^+e^- \to \text{hadrons, non-resonant}) = \sigma(e^+e^- \to q\bar{q}) \cdot \text{Probability}(q\bar{q} \to \text{hadrons}) \tag{1.19a}$$

and

$$\sigma(e^+e^- \to q\bar{q}) = \frac{\pi\alpha^2 Q_q^2}{3E^2}\left[\frac{\beta_q(3 - \beta_q^2)}{2}\right] \tag{1.19b}$$

$$\text{Probability}(q\bar{q} \to \text{hadrons}) = 1 \tag{1.19c}$$

Here Q_q is the magnitude of the quark charge in units of e, that is $Q_q = 1/3$ or $2/3$; and β_q is the quark velocity in units of c, assuming the quark is free and has effective mass M_q. Also $M_q < E$. Hence

$$\sigma(e^+e^- \to \text{hadrons, non-resonant}) = \frac{\pi\alpha^2 Q_q^2}{3E^2}\left[\frac{\beta_q(3 - \beta_q^2)}{2}\right];\ E > M_q \tag{1.20}$$

The term $\pi\alpha^2/3E^2$ in Eq. (1.20) is just Eq. (1.10); and this illustrates the basic nature of the one-photon-exchange production of fermion pairs discussed in Section 1B. Indeed it has become conventional to define

$$R(e^+e^- \to \text{hadrons}) = \sigma(e^+e^- \to \text{hadrons})/\sigma(e^+e^- \to \mu^+\mu^-)$$

where we use the asymptotic value of $\sigma(e^+e^- \to \mu^+\mu^-)$, Eq. (1.10). Thus

$$R(e^+e^- \to \text{hadrons, non-resonant}) = Q_q^2\left[\frac{\beta_q(3 - \beta_q^2)}{2}\right] \tag{1.21a}$$

and for $E \gg M_q$

$$R(e^+e^- \to \text{hadrons, non-resonant}) = Q_q^2\ ,\quad E \gg M_q \tag{1.21b}$$

Basic Model: Resonant Production: At some energies the $q\bar{q}$ form a tightly bound system which constitutes an hadronic resonance. The final state, strong interaction between the quarks cannot be ignored here; indeed the resonance is the final state interaction and it dominates the production cross section. Figure 1.4b illustrates this. Lecture 3 is devoted to a discussion of resonant production of hadrons and so we

return here to the discussion of non-resonant production--often called continuum production of hadrons.

Several Quark Model: For several quarks, all with $M_q \ll E$

$$\sigma(e^+e^- \to \text{hadrons, non-resonant}) = \frac{\pi\alpha^2}{3E^2} \sum_i Q_i^2 \qquad (1.22a)$$

$$R(e^+e^- \to \text{hadrons, non-resonant}) = \sum_i Q_i^2 \qquad (1.22b)$$

In Eqs. (1.22) the summation is over all the different kinds of quarks. Remember that we classify quarks first according to the internal quantum numbers of charge, strangeness, charm and so forth. This leads to the five known types of flavors listed in Table 1.2. In addition each quark flavor comes in three different forms, called colors. These colors do not appear explicitly in particle reactions but must be counted in computing R. Indeed the agreement of the naive quark model for R with the data is the best proof of the three color concept. In Table 1.2, the effective mass is used in comparing M_q with E to see if the particular quark q is produced.

Comparison to Data: Figures 1.5 and 1.6 present measurements of $R(e^+e^- \to \text{hadrons, non-resonant})$.[1.6,1.7] The predictions of the naive quark model. Eqs. (1.22) and Table 1.2, are roughly correct. In making the comparison ignore the ψ/J and Υ narrow resonances and the broad resonances in the $E_{c.m.} = 4$ GeV region.

Improvement to the naive quark model must take account of the quark-antiquark strong interaction in Fig. 1.4a. These days one usually assumes the validity of quantum chromodynamics,[1.9] which predicts

Table 1.2. Properties of known quarks required for calculating $R(e^+e^- \rightarrow \text{hadrons, non-resonant})$.

Name, also called flavor	Symbol	Charge in units of e	Effective mass (GeV/c^2)	Contribution to R including 3 colors per flavor	ΣR as E increases above each M_q
up	u	2/3	0.3 - 0.4	4/3	4/3
down	d	-1/3	0.3 - 0.4	1/3	5/3
strange	s	-1/3	~0.5	1/3	2
charm	c	2/3	1.5 - 1.85	4/3	10/3
bottom	b	-1/3	5.0 - 5.3	1/3	11/3

$$R(e^+e^- \to \text{hadrons; non-resonant}) = \left[\sum_i Q_i^2\right]\left[1 + \frac{\alpha_s(s)}{\pi} + \ldots\right]$$

$$\alpha_s(s) = \frac{12\pi}{33\ \ell n[s/\Lambda^2] + [\text{term dependent on quark mass}]}$$

Here $s = E^2_{c.m.}$ and Λ is a parameter which is taken to lie somewhere between .1 and .7 GeV. The predicted change in R is less than a few tenths. For example at $E_{c.m.} = 5$ GeV $\Delta R = 0.26$ if $\Lambda = .5$ GeV and the quark mass term is ignored. And as $E_{c.m.}$ increases, ΔR decreases. Hence quantum chromodynamics predicts that the naive quark model should be a good model, and it is!

Lecture 2: HEAVY LEPTONS

Positron-electron annihilation physics and heavy lepton physics are intimately connected. The annihilation process is the most direct way of searching for heavy leptons; and the annihilation process is an excellent way of studying leptons so produced. This lecture has seven sections. First, our present concept of a lepton is discussed. Next, various types of heavy leptons are briefly discribed in Sections 2B and 2C. Recent searches for heavy leptons are summarized in Sections 2D and 2E. Finally, selected topics in tau physics are presented.

2A: The Concept of a Lepton

The original concept of a lepton was a spin 1/2, small mass particle (compared to the pion mass) which did not interact through the strong force. The discovery of the tau lepton (mass = 1782 MeV/c^2) removed the mass restriction; and other experiments have elaborated the concept.

I'll first list the elements of the conventional concept; and then discuss possible deviations.

Conventional Concept of a Lepton: At present we call a particle a lepton if:

(a) the particle does not interact through the strong interactions;

(b) the particle interacts through the weak interactions;

(c) the particle has no internal structure and no internal constituents;

(d) there is a particle-type conservation law associated with the particle; and

(e) the spin of the particle is 1/2.

Possible Deviations from the Conventional Concept: Requirements (a) and (b) are intrinsic to the concept of a lepton. For example, a particle without strong and without weak interactions would be an "electromagnetic" particle like the photon.

Requirement (c) says that the lepton must be a point particle; its spatial extent is entirely due to the range of the forces through which it interacts. All the known leptons fulfill the point particle requirements. However we can conceive of a lepton with structure or with internal constituents, that is, a composite lepton.[2.1] It would then act like a proton in reactions; would have a non-unit form factor; but would still satisfy a particle-type conservation law. However the idea of a composite lepton raises the question of what holds the composite lepton together, since the lepton does not have the strong force. (In the hadrons the strong force is intimately connected with their composite nature.) It is then necessary to assume the existence of a new force.

This force must be very strong and must have a very short range so that it, and its effects, remain undetected by present experiments.

Requirement (d) is exemplified by the sequential lepton model, Section 2B. A weaker form of lepton-type conservation is the excited electron (e^*) model, Section 2C. Here the e^{*-} has the same lepton number as the e^-; so that the same lepton number is carried by the ν_e, e^-, and e^{*-}. However one can violate requirement (d) and conceive of a lepton without a lepton-type conservation property. For example, a large mass ℓ^+ lepton might decay via $\ell^+ \rightarrow$ proton + γ. Yet if the ℓ^+ obeyed requirements (a), (b), (c), and (e), we would still call it a lepton.

Requirement (e), the spin being 1/2, is not essential. Indeed in Section 2C we discuss spin 0 leptons predicted by some supersymmetry schemes. However if we remove requirements (d) and (e), then we have no way to distinguish a lepton from the proposed $W^{\pm}$ and Z^o intermediate bosons; since the $W^{\pm}$ and Z^o satisfy requirements (a), (b), and (c).

Obviously, the concept of a lepton is empirical; we should keep the concept general so that our search for new leptons is general.

2B: The Sequential Lepton Model

The Model: In this model[2.2] one assumes there is a mass sequence of charged leptons, each lepton type having a separately conserved lepton number and a unique associated neutrino. This model was instrumental in finding the tau lepton;[2.3] and the electron, muon, and tau are sequential leptons according to all recent measurements. We visualize a sequence

Charged Lepton	Associated Neutrino
$e^{\pm}$	$\nu_e, \bar{\nu}_e$
$\mu^{\pm}$	$\nu_\mu, \bar{\nu}_\mu$
$\tau^{\pm}$	$\nu_\tau, \bar{\nu}_\tau$
$\ell^{\pm}$	$\nu_\ell, \bar{\nu}_\ell$
.	.
.	.
.	.

(2.1)

The radiative decays $\ell^{\pm} \to e^{\pm} + \gamma$, $\ell^{\pm} \to \mu^{\pm} + \gamma$ are then forbidden; and if the ν_ℓ mass is less than the $\ell^{\pm}$ mass, the following kinds of weak decays can occur:

$$\begin{aligned}
&\ell^- \to \nu_\ell + e^- + \bar{\nu}_e \\
&\ell^- \to \nu_\ell + \mu^- + \bar{\nu}_\mu \\
&\ell^- \to \nu_\ell + \tau^- + \bar{\nu}_\tau \\
&\ell^- \to \nu_\ell + \pi^- \\
&\ell^- \to \nu_\ell + K^- \\
&\ell^- \to \nu_\ell + \rho^- \\
&\ell^- \to \nu_\ell + \text{2-or-more hadrons}
\end{aligned} \tag{2.2}$$

In this case the ν_ℓ is stable.

If the ν_ℓ mass is greater than the $\ell^{\pm}$ mass, the $\ell^{\pm}$ is stable and the following types of weak decays occur:

$$
\begin{aligned}
\nu_\ell &\to \ell^- + e^+ + \nu_e \\
\nu_\ell &\to \ell^- + \mu^+ + \nu_\mu \\
&\;\;\vdots \qquad\quad \vdots \\
\nu_\ell &\to \ell^- + \pi^+ \\
&\;\;\vdots \qquad\quad \vdots \\
\nu_\ell &\to \ell^- + \text{2-or-more hadrons}
\end{aligned}
\tag{2.3}
$$

Branching Ratios and Lifetime: There is an easy way to crudely calculate the branching ratios and lifetime of a sequential lepton. Consider the case where m_ℓ, the $\ell^\pm$ mass, is greater than m_{ν_ℓ}, the ν_ℓ mass. And suppose

$$m_\ell - m_{\nu_\ell} >> m_i \tag{2.4a}$$

where i = e, μ, τ; u quark, d quark, s quark, c quark. Then as shown in Fig. 2.1, the W^- from the $\ell^- - \nu_\ell$ vertex can convert to the following pairs: $e^-\bar{\nu}_e$, $\mu^-\bar{\nu}_\mu$, $\tau^-\bar{\nu}_\tau$, $\bar{u}d$, and $\bar{c}s$. The weak coupling of each of these pairs to the W^- is the same; however the quarks have three colors which contribute a relative weight of 3. Therefore the branching fractions are:

$$
\begin{aligned}
&B(\ell^- \to \nu_\ell e^-\bar{\nu}_e) = B(\ell^- \to \nu_\ell \mu^-\bar{\nu}_\mu) = B(\ell^- \to \nu_\ell \tau^-\bar{\nu}_\tau) = 1/9 \\
&B(\ell^- \to \nu_\ell \text{ hadrons}) = 2/3
\end{aligned}
\tag{2.4b}
$$

Here all lepton and quark masses in the final state have been ignored after using the restriction in Eq. (2.4a).

As another example consider the τ^- decay where only $e^-\bar{\nu}_e$, $\mu^-\bar{\nu}_\mu$, and $\bar{u}d$ pairs can be produced. The predicted branching ratios are

$$B(\tau^- \to \nu_\tau e^-\bar{\nu}_e) = B(\tau^- \to \nu_\tau \mu^-\bar{\nu}_\mu) = 0.20 \tag{2.5}$$

Measurement yields 0.17 for these ratios,[2.4] which is quite good for such a crude method.

More precise branching ratio calculations[2.5] require either empirical or theoretical knowledge of how the W^- couples to hadrons.

Next I consider the lifetime of the $\ell^\pm$. The decay width for $\ell^- \to \nu_\ell e^-\bar{\nu}_e$ can be calculated directly using conventional weak interaction theory[2.6]

$$\Gamma(\ell^- \to \nu_\ell e^-\bar{\nu}_e) = \frac{G^2 m_\ell^5}{192\ \pi^3} \tag{2.6}$$

Here the e mass has been ignored, and G is the Fermi coupling constant, 1.17×10^{-5} GeV^{-2}. Then the lifetime is

$$T_\ell = 1/\Gamma(\ell^- \to \text{all}) = B(\ell^- \to \nu_\ell e^-\bar{\nu}_e)/\Gamma(\ell^- \to \nu_\ell e^-\bar{\nu}_e) \tag{2.7}$$

It is convenient to relate this to the μ lifetime

$$T_\mu = 2.2 \times 10^{-6} \text{ sec} = 1/\Gamma(\mu^- \to \nu_\mu e^-\bar{\nu}_e)$$

Then

$$T_\ell = 2.2 \times 10^{-6}\ B(\ell^- \to \nu_\ell e^-\bar{\nu}_e)(m_\mu/m_\ell)^5 \tag{2.8}$$

Hence T_ℓ decreases rapidly as m_ℓ increases. For the τ

$$T_\tau(\text{predicted}) = 2.7 \times 10^{-13} \text{ sec} \tag{2.9}$$

Present measurements[2.7] give an upper limit of 1.4×10^{-12} sec.

All of the section assumes $m_\ell > m_{\nu_\ell}$. If $m_{\nu_\ell} > m_\ell$, the same considerations hold, and there are identical branching ratio and lifetime formulas for the ν_ℓ.

2C: Other Varieties of Heavy Leptons

In this section I will give some examples of other possible varieties of heavy leptons.[2.6]

Excited Leptons: In one model, called the ortholepton[2.6] model, the charged lepton is assigned the same lepton number as the same sign e, μ or τ; and there is no additional neutrino. For example, we conceive of a particle e^* which may be thought of as an excited e. Then

$$e^{*\pm} + e^{\pm} + \gamma \tag{2.10}$$

will be the dominant decay mode unless we suppress the $e^* - \gamma - e$ coupling. We can also conceive of a heavy neutral lepton with the same lepton number as the e, μ, or τ; really a heavy neutrino. Typical decay modes would be

$$\begin{aligned} \ell^o &\to e^- + (\text{hadrons})^+ \\ \ell^o &\to \nu_e + (\text{hadrons})^o \end{aligned} \tag{2.11}$$

Paraleptons: In this model[2.8,2.9] we conceive of a particle E^+ or M^+ which has the lepton number of the e^- or μ^- respectively. This association of lepton number with opposite electric charge prevents radiative decays such as $E^+ \not\to e^+ + \gamma$. Hence, such charged leptons decay through the weak interactions. For example

$$\begin{aligned} E^- &\to \bar{\nu}_e + e^- + \bar{\nu}_e \\ E^- &\to \bar{\nu}_e + \mu^- + \bar{\nu}_\mu \\ E^- &\to \bar{\nu}_e + \text{hadrons} \end{aligned} \tag{2.12}$$

Stable Heavy Leptons: Of course we can devise heavy leptons, charged or neutral, which have no partners or relatives with the same lepton number. These would be stable if their lepton number were conserved.

Spin 0 Leptons from Supersymmetry Proposals: Theories which connect bosons and fermions, the supersymmetry theories, may propose[2.10] spin 0 leptons. For example consider the following scheme[2.10]

Normal Particle		Supersymmetric Partner	
particle	spin	particle	spin
e^-	1/2	e_s^-	0
γ	1	γ_s (photino)	1/2

(2.13)

where the e^- and e_s^- have the same lepton number. If $m_{e_s} > m_e$, the dominant decay mode is

$$e_s^- \to e^- + \gamma_s \tag{2.14}$$

Spin > 1/2 Leptons: As discussed in Section 2A we can think about leptons of arbitrary spin. However for spin > 1/2 a problem occurs with the reaction

$$e^+ + e^- \to \ell^+ + \ell^- \tag{2.15}$$

at very high energy. By itself, the one-photon exchange diagram, Fig. 2.2a yields a $\sigma(e^+e^- \to \ell^+\ell^-)$ which violates the unitarity limit on σ. For example,[2.11] if the spin is 3/2

$$\sigma(e^+e^- \to \ell^+\ell^-) \sim \frac{\alpha^2 E^2}{m_\ell^4} \tag{2.16}$$

which contradicts

$$\sigma(e^+e^- \to \ell^+\ell^-) \leq \frac{\text{constant}}{E^2} \tag{2.17}$$

at sufficiently high energy. This problem can be avoided in two ways:

(a) There must be other diagrams which cancel the higher power terms in E. This is what happens in the process $e^+ + e^- \to W^+ + W^-$ (see Section 4C).

(b) Alternatively, the leptons must have a form factor which decreases sufficiently rapidly as E increases.

2D: Searches for Heavy Leptons Not Using e^+e^- Annihilation

Hadron + Hadron Collisions: This process[2.12] offers the highest energy for producing new leptons, particularly when the $\bar{p}$ + p and p + p colliding beams facilities now being built are available. Unfortunately there are no definitive signatures for most of the lepton types discussed in the last two sections; and the backgrounds are very large.[2.12] So far this production method has been most effective in searching for long-lived or stable leptons,[2.13] but none have been found.

Photon + Hadron Collisions: The Bethe-Heitler process

$$\gamma + \text{nucleus} \to \ell^+ + \ell^- + \text{anything} \qquad (2.18)$$

seems to be a somewhat more fruitful way to search[2.14] for new charged leptons. However there are still enormous backgrounds; and the only feasible search method[2.15] is to select events in which the "anything" in Eq. (2.18) has very low multiplicity and $\ell^+ \to e^+ + \nu$'s, $\ell^- \to \mu^- + \nu$'s or vice versa. That is, $\mu^\pm e^\mp$ is the ℓ pair production signature. However even this is very difficult as is demonstrated by the fact that the τ has not yet been detected by this method because charmed particles produce a $\mu^\pm e^\mp$ signal that is several orders of magnitude larger.

ν - Hadron Collisions: If a new charged lepton couples to a ν_μ, $\bar{\nu}_\mu$, ν_e, $\bar{\nu}_e$, ν_τ or $\bar{\nu}_\tau$ then the production reaction

$$\nu + \text{nucleon} \rightarrow \ell^{\pm} + \text{anything} \tag{2.19}$$

can occur.[2.16] The cross section depends upon the mass of the ℓ, the ν energy, and the strength of the coupling of the ν to the ℓ lepton. Since in general we expect no coupling between a ν and an arbitrary lepton, this is a very restrictive search method. But if there is a new ℓ which couples to a ν this is a powerful search method.

Thus charged lepton search methods at proton accelerators are either very difficult or very restrictive.

2E. Searches for Heavy Leptons Using e^+e^- Annihilation

Charged Leptons: The one-photon-exchange process, Fig. 2.2a, is the most definitive way[2.17] to search for charged leptons. It is effective for sequential charged leptons, excited charged leptons, paraleptons, stable charged leptons, and for charged leptons of any spin. When $E >> m_\ell$ the production cross sections are

$$\begin{aligned} \sigma(e^+e^- \rightarrow \ell^+\ell^-) &= \frac{\pi\alpha^2}{12E^2}; \quad \text{spin} = 0 \\ \sigma(e^+e^- \rightarrow \ell^+\ell^-) &= \frac{\pi\alpha^2}{3E^2}; \quad \text{spin} = 1/2 \end{aligned} \tag{2.20}$$

And the respective values of R are 1/4 and 1.

The use of the e^+e^- annihilation process was first suggested in 1967 by Zichichi et al.[2.18] Searches were carried out by that group[2.19] and by Orito et al.[2.20] using the ADONE e^+e^- storage ring at Frascati. A lower limit of 1.0 to 1.2 GeV/c^2 was set on the mass of a heavy charged

lepton. Subsequently the e^+e^- annihilation process was used to discover the τ and study its properties in the period 1974-1980.[2.3]

No charged heavy leptons other than the τ have been found. Table 2.1 gives the current lower limits on the masses for various kinds of charged leptons.

Neutral Leptons: The definitive way to search for neutral heavy leptons is to use the one-Z^o-exchange process, Eq. (2.21) and

$$e^+ + e^- \to Z^o \to \ell^o + \bar{\ell}^o \qquad (2.21)$$

Fig. 2.2b. Unfortunately this process has a small cross section at existing e^+e^- facilities;[2.17] and the effective use of this search method must await higher energy e^+e^- facilities (see Section 4B and 4C).

2F: The Status of the Tau

General Properties of Tau: Several reviews of the status of the τ have appeared recently;[2.4,2.27] and I will simply summarize that status. To the best of our knowledge the τ is a spin 1/2, charged, sequential lepton; it is a point particle; it obeys conventional quantum electrodynamic theory via the Dirac equation; and it obeys conventional weak interaction theory with V-A coupling for the $\tau - \nu_\tau$ vertex.

The τ mass is 1782^{+3}_{-4} MeV/c^2 and all measured properties are consistent with that mass. Its lifetime, for example, is measured to be less than 1.4×10^{-12} sec;[2.7] and for that mass a lifetime of 2.7×10^{-13} sec is predicted.

Point Particle Nature of Tau: We test the point particle nature of the τ by measuring if the cross section for

$$e^+ + e^- \to \tau^+ + \tau^- \qquad (2.22)$$

Table 2.1. Present lower limits on the masses of new charged leptons from e^+e^- searches.

Lepton type	Lower limit on mass (GeV/c^2)	References and comments
sequential $\ell^{\pm}$	13.0 to 17.0	Results from JADE, MARK J, PLUTO, TASSO at PETRA. The 17 GeV/c^2 limit is from JADE. Ref. 2.21
stable $\ell^{\pm}$	12.0	JADE at PETRA, Ref. 2.22
spin 0 super-symmetry electron $e_s \rightarrow e$ + photino	13.0 to 16.0	The 16 GeV/c is from JADE at PETRA, Ref. 2.23; the 13 GeV/c is from PLUTO at PETRA, Ref. 2.24
excited electron e^* with $e^* \rightarrow e + \gamma$ or excited muon μ^* with $\mu^* \rightarrow \mu + \gamma$	3.0	SPEAR Ref. 2.25 ADONE Ref. 2.26

is consistent with

$$\sigma(e^+e^- \to \tau^+\tau^-) = \frac{\pi\alpha^2}{3E^2}\left[\frac{\beta(3-\beta^2)}{2}\right] \tag{2.23}$$

From threshold to about $E_{c.m.} = 7$ GeV that behavior has been established at SPEAR[2.4,2.27,2.28] and DORIS.[2.4,2.27] At higher energies, PETRA experiments[2.7,2.24,2.29] have verified Eq. (2.23) for the τ. Table 2.2 gives the data in terms of the $\Lambda_{\pm}$ QED breakdown parameters of Eq. (1.13a). Thus all measurements are consistent with the τ being a point particle.

G_τ and the τ Lifetime: We have been assuming that the Fermi weak interaction coupling constant, G_τ, for the $\tau - \nu_\tau$ coupling, is equal to the universal Fermi constant G. But there is no proof of this. There are three ways to measure G_τ:

(a) The decay width of a heavy meason

$$M^- \to \tau^- + \nu_\tau \tag{2.24}$$

is proportional to G_τ.

(b) The charge current cross section for the interaction of a tau neutrino, ν_τ, with nucleons

$$\nu_\tau + N \to \tau^- + \text{anything} \tag{2.25}$$

is also proportional to G_τ

(c) All the partial decay widths for τ decays are proportional to G_τ. For example Eq. (2.6) should be written

$$\Gamma(\tau^- \to \nu_\tau e^-\bar{\nu}_e) = \Gamma(\tau^- \to \nu_\tau \mu^-\bar{\nu}_\mu) = \frac{G_\tau G m_\tau^5}{192\,\pi^3} \tag{2.26}$$

Then Eqs. (2.8) and (2.9) become

$$T_\tau = 2.2 \times 10^{-6}\ B(\tau^- \to \nu_\tau e^-\bar{\nu}_e)\left(\frac{m_\mu}{m_\tau}\right)^5\left(\frac{G}{G_\tau}\right) \tag{2.27}$$

Table 2.2. Lower limits on $\Lambda_{\pm}$ breakdown parameters at 95% confidence level for $e^+e^- \to \tau^+\tau^-$, from PETRA experiments.

Detector	Lower limit on		Reference
	Λ_+ (GeV)	Λ_- (GeV)	
Mark J	76	157	2.29
PLUTO	74	65	2.24
TASSO	67	74	2.7

$$T_\tau = 2.7 \times 10^{-13}\left(\frac{G}{G_\tau}\right) \tag{2.28}$$

The current upper limit[2.7] of 1.4×10^{-12} sec yields

$$G_\tau/G > 0.19 \tag{2.29}$$

Method (a) suffers from uncertainties in the decay mechanism of the M as discussed in Section 2F. Method (b) requires the production of a known flux of ν_τ's; also discussed in Section 2F. The measurement of T_τ, method (c), is the most feasible way at present to measure G_τ. J. Jaros[2.30] has devised a method using $e^+e^- \to \tau^+\tau^-$ to measure T_τ to $\lesssim 20\%$ precision. Bubble chamber measurements of T_τ using $\nu_\tau + N \to \tau^- + X$ have also been proposed.[2.31,2.32]

The Tau Neutrino: Our knowledge of the tau neutrino, ν_τ, is still incomplete. Its mass is less than 250 MeV/c^2. This upper limit has been obtained in two ways: by studying[2.28] the e^- momentum spectrum in the decay $\tau^- \to \nu_\tau + \bar{\nu}_e + e^-$; and by studying[2.33] the π^- momentum spectrum in the decay $\tau^- \to \nu_\tau + \pi^-$. However at present we don't know if the ν_τ mass is zero or close to zero, as are the ν_e and ν_μ masses.

The ν_τ has been shown to be different[2.4,2.27] from the $\bar{\nu}_e$, ν_μ, and $\bar{\nu}_\mu$. However it is possible that the ν_τ and ν_e are the same particle. In that case the τ would be an ortholepton (Section 2C) and the decay mode

$$\tau^- \to e^- + \gamma \tag{2.29}$$

would have to be strongly suppressed by an unknown mechanism. I say strongly because the measured upper limit on the branching fraction for $\tau \to e^- + \gamma$ is 6.4×10^{-4} with a 90% C.L.[2.25]

2G: Prospects for Tau Neutrino Physics

The incompleteness of our knowlege of the tau neutrino has led to strong interest in doing experiments with tau neutrinos. One would like to determine if the interaction of the ν_τ with nucleons obeys conventional weak interaction theory; for example, does $G_\tau = G$? And one would like to distinguish the ν_τ from the ν_e definitively, if they are indeed different particles. A more speculative objective is to look for neutrino oscillations occurring through the mixing of neutrinos.[2.34]

The only known method[2.35-2.37] for producing a ν_τ beam is the production and decay sequence

$$\text{proton} + \text{nucleon} \rightarrow F^- + \text{hadrons} \tag{2.30}$$

$$F^- \rightarrow \tau^- + \bar{\nu}_\tau \tag{2.31}$$

$$\tau^- \rightarrow \nu_\tau + \text{charged particles} \tag{2.32}$$

Here F is the charmed meson containing $c\bar{s}$ quarks. The neutrinos from π and K decay would overwhelm the ν_τ signal unless the majority of the π's and K's interact before they decay. Therefore the entire proton beam must be dumped in a thick target, Fig. 2.3. There is still some problem with ν_e's and ν_μ's from D meson and other charmed particle semi-leptonic decays, but the detection of the ν_τ appears feasible.

Experiments using ν_τ beams so produced become easier as the primary proton beam energy increases. Therefore a number of proposals[2.31,2.32,2.38] have been made to the Fermi National Laboratory to do ν_τ experiments using the 1000 GeV tevatron proton beam. Some of the current lower energy neutrino beam dump experiments at Fermilab[2.39] and CERN[2.40] may be able to detect ν_τ events.

There are two uncertainties in the calculation of the ν_τ flux. First, the cross section for F production in Eq. (2.30) is probably of the order of magnitude of D production; but we don't know the F production cross section to within a factor of 3. The second uncertainty is in the branching fraction $B(F^- \to \tau^- \bar{\nu}_\tau)$. It depends upon the lifetime of the F, T_F, and on

$$\Gamma(F^- \to \tau^- \bar{\nu}_\tau) = \frac{G^2 f_F^2 m_F m_\tau^2}{8\pi} \left(1 - \frac{m_\tau^2}{m_F^2}\right)^2 \tag{2.33}$$

Here G is the Fermi coupling constant; m_F is the F mass; m_τ is the τ mass; and f_F is a parameter in units of energy which depends upon the detailed mechanism for

$$F^- \to \tau^- + \bar{\nu}_\tau \tag{2.34}$$

This formula and the f_F parameter are analogous to the formula and f_π parameter[2.6] for

$$\pi^- \to \mu^- + \bar{\nu}_\mu \tag{2.35}$$

In π decay $f_\pi \approx 0.1$ GeV; f_F is very probably larger than this by a factor of 2 to 4. But we don't know how to calculate f_F precisely. The uncertainty in f_F, which enters as the square; and the uncertainty in the current measurements of T_F[2.41] lead to a large uncertainty in

$$B(F^- \to \tau^- \bar{\nu}_\tau) = \Gamma(F^- \to \tau^- \bar{\nu}_\tau) T_F \tag{2.36}$$

Indeed estimates of the branching ratio range from 0.5 to 20%! (The proposed ν_τ beam dump experiments are quite feasible as planned if the ratio is at least 3%.)

Lecture 3: QUARKONIUM AND e^+e^- ANNIHILATION

In this lecture I will introduce you to another aspect of e^+e^- annihilation physics--the production and properties of the resonant, heavy, $q\text{-}\bar{q}$ systems produced in e^+e^- annihilation, namely the ψ/J and Υ particle families. We shall see that some beautiful non-relativistic quantum mechanics provide a basic understanding of these systems.

Since I will do this introduction in a single lecture, I will limit my discussion to the static properties of $q\text{-}\bar{q}$ systems with the quantum numbers of the photon. These systems are directly produced by

$$e^+ + e^- \to q\text{-}\bar{q} \text{ resonance} \tag{3.1}$$

References 3.1-3.4 present much fuller accounts of this subject.

3A: General Properties of $e^+e^- \to$ Resonance

Figure 1.4b illustrates the general diagram

$$e^+ + e^- \to \text{resonance } V \to \text{final state f.} \tag{3.2}$$

We use V to designate the resonance because it must have spin 1, and hence be a vector particle, like the photon. The final state f can be hadrons or a lepton-antilepton pair such as e^+e^-, $\mu^+\mu^-$, $\tau^+\tau^-$, $\nu_e\bar{\nu}_e$, $\nu_\mu\bar{\nu}_\mu$, ...

The non-relativistic Breit-Wigner formalism[3.5] gives

$$\sigma(e^+e^- \to V \to f) = \frac{3\pi}{s} \frac{\Gamma_{ee}\Gamma_f}{(E_{c.m.} - M_V)^2 + \Gamma^2/4} \tag{3.3}$$

Here $s = E^2_{c.m.}$; Γ is the total decay width of the V; Γ_{ee} is the partial decay width for $V \to e^+e^-$; Γ_f is the partial decay width for $V \to f$; M_V is the mass of the V. Figure 3.1a shows the shape of this resonance. This equation ignores threshold effects, the energy spread of the e^+ and

e^- colliding beams, and corrections for the effect of radiating undetected photons.

The description of a resonance thus requires the determination of M_V, Γ, Γ_{ee}, and the various other Γ_f's. Usually the Γ_f's other than Γ_{ee} are determined by measuring

$$B(V \to f) = \Gamma_f/\Gamma \tag{3.4}$$

In e^+e^- annihilation it is customary to study the total hadronic cross section

$$\sigma(e^+e^- \to V \to \text{hadrons}) = \frac{3\pi}{s} \frac{\Gamma_{ee}\Gamma_{had}}{(E_{c.m.} - M_V)^2 + \Gamma^2/4} \tag{3.5}$$

where

$$\Gamma_{had} = \sum_{\substack{\text{all hadronic} \\ \text{final states}}} \Gamma_f \tag{3.6}$$

The known resonance produced via $e^+e^- \to V$ all have $\Gamma_{had} > .85\Gamma$. Therefore we use the simplificative approximation

$$\Gamma_{had} \approx \Gamma \tag{3.7}$$

Hence

$$\sigma(e^+e^- \to V \to \text{hadrons}) \approx \frac{3\pi}{s} \frac{\Gamma_{ee}\Gamma}{(E_{c.m.} - M_V)^2 + \Gamma^2/4} \tag{3.8a}$$

Using the definition of R introduced in Sec. 1C

$$R(e^+e^- \to V \to \text{hadrons}) \approx \frac{9}{4\alpha^2} \frac{\Gamma_{ee}\Gamma}{(E_{c.m.} - M_V)^2 + \Gamma^2/4} \tag{3.8b}$$

Thus the position of V yields M_V; the width of V yields Γ; and the maximum height

$$R_{max} = R(E_{c.m.} = V) = \frac{9}{\alpha^2}\frac{\Gamma_{ee}}{\Gamma} \tag{3.9}$$

yields Γ_{ee}, as shown in Fig. 3.1a.

Often the energy spread of the e^+ and e^- beams is as large as, or larger than, Γ. Then, as shown in Fig. 3.1b

$$\begin{aligned} \Gamma_{observed} &> \Gamma \\ R_{max,observed} &< R_{max} \end{aligned} \tag{3.11}$$

Then we measure

$$\int R(e^+e^- \to V \to \text{hadrons})\, dE \approx \frac{9\pi}{2\alpha^2}\Gamma_{ee} \tag{3.12}$$

using Eq. (3.7). Hence the area under the resonance determines Γ_{ee}. Then one measures separately $B(V \to e^+e^-)$ to determine

$$\Gamma = \Gamma_{ee}/B(V \to e^+e^-) \tag{3.13}$$

Equation (3.12) shows that Γ_{ee} is a measure of the area under a resonance.

3B: The Directly Produced ψ/J and T Resonance Families

Naive Quark Model of Mesons: The naive quark model of the mesons assumes

(a) A meson consists of one quark plus one antiquark.

(b) The internal quantum numbers of the quark are additive.

(c) The mass of a meson is given by the sum of the masses of the quark and antiquark reduced by the quark-antiquark binding energy.

For a meson composed of a quark and its own antiquark, the spin-parity rules of positronium apply. Defining S = total spin = 0,1; L = orbital angular momentum; J = total angular momentum:

$$P = \text{parity} = -(-1)^{L}$$
$$C = \text{charge conjugation number} = (-1)^{L+S} \tag{3.14}$$

And there are two spin states for each L state, a triplet state with J = 1 and a singlet state with J = 0. The resonances produced via Eq. (3.1) have the quantum numbers of the photon: J = 1, P = -1, C = -1. Hence the states which are produced directly via Eq. (3.1) have

$$S = 1,\ J = 1,\ L = 0,\ 2,\ 4\ \ldots \tag{3.15}$$

For fixed radial excitation quantum number (see the next section); L = 0, that is the S state, is the lowest energy state. And it is these $^3S_1$ states in the ψ/J and Υ families which will concern us for the remainder of the lecture.

We are about to plunge into one part of the vast subject of quarkonium. And before doing so I must provide some basic references for the reader who wishes to explore this subject or who wishes to read the detailed arguments from data and theory about the properties of quarkonium. The ψ/J particles are states of the $c\text{-}\bar{c}$ system. The ψ/J itself was discovered concurrently in e^+e^- annihilation[3.6] at SPEAR; and through the hadron reaction[3.7]

$$p + \text{Nucleus} \rightarrow J + \text{anything}$$
$$J \rightarrow e^+ + e^- \tag{3.16}$$

at BNL. Almost all of the studies of the ψ/J family have used e^+e^- annihilation. Reference 3.8 presents a comprehensive review of the experimental method and the data for this family.

The Υ family are states of the $b\text{-}\bar{b}$ system, and the family was first discovered at Fermilab through the reaction[3.9]

$$p + \text{Nucleus} \rightarrow \Upsilon + \text{anything}$$
$$\Upsilon \rightarrow \mu^+ + \mu^- \tag{3.17}$$

However, as with the ψ/J family, most studies have been done using e^+e^- annihilation at DORIS[3.10] and CESR.[3.11]

Table 3.1 gives some of the parameters of the ψ/J and Υ particles with $^3S_1$ structure. I have included the ρ for comparison purposes; its quarks are too light to be treated non-relativistically. The ψ'' is mostly a $^3D_1$ state and is also included for comparison purposes. The $R_{max,observed}$ values are usually dependent on the storage ring used; they are not of fundamental interest.

3C: Non-relativistic Potential Model of Heavy $q-\bar{q}$ Systems

Energy Levels and Mass: In this non-relativistic model the masses of a $q-\bar{q}$ system are given by

$$M_{q-\bar{q}} = 2\, m_q + E_b \tag{3.18}$$

Here m_q is the mass of the q quark; and E_b is the binding energy and is negative.

In this lecture I ignore all effects on E_b from spin-orbit coupling, from spin-spin coupling, from tensor coupling, and from relativistic corrections. These effects are important;[3.1-3.4] indeed the spin effects lead to the fine structure and hyperfine structure in the energy levels.

The binding energy, E_b, is given by the Schrödinger equation

$$-\frac{1}{2\mu}\nabla^2\psi(r) + V(r)\,\Psi(r) = E_b\,\Psi(r) \tag{3.19}$$

where $\mu = m_q/2$ is the reduced quark mass.

Table 3.1. Parameters of the ρ, ψ/J family and T family. The ρ and ψ/J parameters are taken from Ref. 3.12. The T parameters are from Ref. 3.11; and CLEO detector mass measurements are used for consistency. This table is pedagogical. 3.8, 3.11 and 3.12 should be used for information on the errors and on the differences between measurements. When $R_{max,observed}$ is dependent on the e^+e^- storage ring used, the ring is indicated.

V	Spectroscopic State	$q\bar{q}$ Constant	Mass (MeV)	Γ_{ee} (KeV)	Γ (KeV)	$B(V \to ee)$	$R_{max,calculated}$	$R_{max,observed}$
ρ	$^3S_1$	$\frac{1}{\sqrt{2}}(u\bar{u} + d\bar{d})$	776	6.8	158000	4.3×10^{-5}	7.3	~7
ψ/J	$^3S_1$	$c\bar{c}$	3097	4.4	63	0.07	10200.	~260 (SPEAR)
ψ'	$^3S_1$	$c\bar{c}$	3685	1.9	215	0.009	1490.	~95 (SPEAR)
ψ''	$^3D_1$	$c\bar{c}$	3768	0.3	25000	1.3×10^{-5}	2.2	~2 (SPEAR)
T	$^3S_1$	$b\bar{b}$	9434	~1.1	~40	~0.03	~5000	~18 (CESR)
T'	$^3S_1$	$b\bar{b}$	9995	~0.5	?	?		~7 (CESR)
T''	$^3S_1$	$b\bar{b}$	10324	~0.3	?	?		~6 (CESR)
T'''	$^3S_1$	$b\bar{b}$	10548	0.22	19000	1.1×10^{-5}	1.8	~1 (CESR)

The potential V(r) is selected to meet two requirements:

(a) At short distances V(r) should be coulomblike to represent gluon exchange.

(b) At large distances the potential should confine the quarks.

A convenient pedagogical choice, with a long history,[3.1] is

$$V(r) = -\frac{b}{r} + ar \quad ; \quad b > 0 \, , \, a > 0 \tag{3.20}$$

The linear potential term, ar, confines the quarks.

We find the energy levels of this potential by calculating the energy levels for each term separately; and then interpolating between them. An alternate pedagogical approach[3.4] uses the three-dimensional harmonic oscillator potential, $kr^2/2$, instead of the linear potential to confine the quarks, and then interpolates.

Coulomb Potential: Figure 3.2a shows the well-known energy levels of the coulomb potential. The neglect of all spin effects leads to the degeneracy of energy levels. I have labelled the levels with an integer quantum number $\hat{n}$ which is different from the usual total quantum number n. The latter gives the energy eigenvalues $E_n = -\mu e^4/2n^2$; while $\hat{n}$ is the number of times R(r) = 0 where R(r) is the radial wave function. In computing $\hat{n}$ the $r = \infty$ point is included but the r = 0 point is excluded. Figure 3.3 illustrates this. The importance of using $\hat{n}$ is that in interpolating between potentials the number of R(r) = 0 points of a wave function is a constant.

Linear Potential: The energy levels of the linear potential, Fig. 3.2b, are pedagogically interesting because there is no degeneracy. Unfortunately the calculations must be done numerically.[3.1] In Fig. 3.2, the $\hat{1}$s to $\hat{2}$s spacing has been set to be the same for both potentials.

Coulomb + Linear Potential: Figure 3.4 interpolates between the two potentials. Our next task is to look at the ψ/J and Υ energy levels to see qualitatively how this potential mixture fits the data. As I said before, we shall restrict our attention to the $\hat{n}\,^3S_1$ states, which we shall denote simply by $\hat{n}S$.

3D: Fitting the ψ/J and Υ $^3S_1$ States.

The Data: Figure 3.5 shows the measured masses, and hence the energy levels, of the $\hat{n}S$ states. It is drawn so that the $\hat{1}S$ states coincide. The Γ_{ee} values are also given. There are four observations:

(a) The spacing between $\hat{1}S$ and $\hat{2}S$, ΔE_{12}, is roughly independent of the quark mass, m_q.

(b) In the Υ system the level spacing, ΔE, decreases as $\hat{r}$ increases.

(c) Γ_{ee} decreases as $\hat{n}$ increases.

(d) $\Gamma_{ee}(\Upsilon)$ is about 1/4 of $\Gamma_{ee}(\psi/J)$.

We show next how the potential

$$V(r) = -\frac{b}{r} + ar \tag{3.21}$$

qualitatively explains these observations.

Effect of Quark Mass on ΔE_{12}: Consider a power-law potential $V(r) = Ar^\nu$ and make the variable change $\rho = r\mu^{-\alpha}$ in the Schrödinger equation. Recall, μ is the reduced quark mass. Then Eq. 3.19 becomes

$$\frac{-1}{2\mu^{2\alpha+1}}\nabla_\rho^2\Psi + A\mu^{\alpha\nu}\rho^\nu\Psi = E\Psi$$

or

$$-\frac{1}{2}\nabla_\rho^2\Psi + A\mu^{\alpha\nu+2\alpha+1}\rho^\nu\Psi = \mu^{2\alpha+1}E\Psi$$

If we set $\alpha\nu + 2\alpha + 1 = 0$ and define

$$E' = \mu^{\nu/(2+\nu)} E$$

We obtain a mass independent equation

$$-\frac{1}{2}\nabla_\rho^2 \Psi + A\rho^\nu \Psi = E'\Psi \tag{3.22}$$

Hence

$$\Delta E \text{ scales as } \mu^{-\nu/(2+\nu)} \tag{3.23a}$$

$$\Delta E \text{ scales as } \mu, \qquad \text{coulomb} \tag{3.23b}$$

$$\Delta E \text{ scales as } \mu^{-1/3} \qquad \text{linear} \tag{3.23c}$$

Thus observation a., the insensitivity of ΔE_{12} to μ, can be explained by a potential which interpolates between coulomb and linear.

Decrease of ΔE With Increasing $\hat{n}$: Figure 3.4 predicts observation b.

Γ_{ee} Decreases as $\hat{n}$ increases: Here we call upon the van Royen-Weisskopf formula[3.2,3.14]

$$\Gamma_{ee} = \frac{16\pi\, Q_q^2\, \alpha^2}{M_V^2} \left|\Psi(o)\right|^2 \quad ; \tag{3.24}$$

Q_q is the quark charge and $\Psi(o)$ is Ψ at $r = 0$. For the coulomb potential, a direct calculation from the wave functions[3.13] yields

$$|\Psi_1(o)|^2 : |\Psi_2(o)|^2 : |\Psi_3(o)|^3 = 1 : 1/8 : 1/27 \tag{3.25}$$

Whereas for a linear potential[3.1,3.2] $|\Psi_{\hat{n}}(o)|^2$ is independent of $\hat{n}$. Hence a mixture of coulomb plus linear potential will agree with observation c.

$\Gamma_{ee}(T) \sim \frac{1}{4}\Gamma(\psi/J)$: A crude explanation of observation d. is as follows. For a power-law potential Ar^ν; $|\Psi(o)|^2$ scales as $\mu^{3/(2+\nu)}$ for S states.[3.2] Hence for coulomb, $|\Psi(o)|^2$ scales as μ^3; and for linear as μ. Let's roughly take the potential mixture as scaling as μ^2. Then from Eq. (3.24)

$$\frac{\Gamma_{ee}(T)}{\Gamma_{ee}(\psi/J)} \sim \frac{Q_b^2}{Q_c^2}\,\frac{M_\psi^2}{M_T^2}\,\frac{\mu_b^2}{\mu_c^2} \sim \frac{Q_b^2}{Q_c^2} \sim \frac{1}{4} \tag{3.26}$$

where b and c refer to the bottom and charm quark respectively. Eq. (3.25) should be taken as illustrative rather than quantitative because our estimate of $|\Psi_T(o)|^2 / |\Psi_\psi(o)|^2$ was so rough.

Conclusions: Thus the mixture of a coulomb plus a linear potential can qualitatively, at least, fit the mass differences and the Γ_{ee} values. Indeed a quantitative fit can also be made[3.1,3.2] using

$$V(r)\ (\text{GeV}) \approx -\frac{.1}{r} + 0.9r \quad , \quad r \text{ in fermis} \tag{3.27}$$

This formula illustrates the magnitude and general behavior of the V(r) which is required. However, the important portion of V(r) lies in the region $0.1 < r < 1.0$ fermis; and other more empirical formulas work as well. For example the logarithmic potential

$$V(r)\ (\text{GeV}) = c\ \ell n(r/r_0) \tag{3.28}$$

has been used; and also the form[3.15]

$$V = a + br^\gamma,\ \gamma \sim 0.1 \tag{3.29}$$

works.

The best form for the potential depends upon two additional areas which I do not have the time to discuss:

(a) V(r) must fit other data such as the masses of the $^1S_0$ and $^3P_1$ states; the rates of electromagnetic transitions between states; and so forth.

(b) Relativistic and quantum chromodynamic considerations must be taken into account. Ultimately, one would like to derive V(r) from quantum chromodynamics.[3.16] The reader must go to Refs. 3.1 to 3.4 for further discussion.

Lecture 4: e^+e^- PHYSICS AT VERY HIGH ENERGY

In the first three lectures I discussed physics which has been done and which can be done at existing e^+e^- facilities. In this fourth and final lecture I discuss the prospects for e^+e^- physics at total energies above 45 GeV, that being the maximum energy attainable by the existing e^+e^- storage rings. The subjects which I emphasize are:

(a) the conventional theory of e^+e^- annihilation through the weak interactions;

(b) the production and study of the expected Z^o and $W^\pm$ intermediate vector bosons; and

(c) the capabilities and limitations of e^+e^- colliding beams storage rings and colliding beams linear accelerators.

4A: e^+e^- Annihilation Through the Weak Interactions

Before assuming the existence of the Z^o intermediate boson required in conventional weak interaction theory, let's look at the old four-fermion, point interaction theory of Fermi. After all, the Z^o has not been discovered yet; and we should be prepared for some surprises at very high energies. In the first part of this lecture I use the simplest example--$e^+e^- \to \mu^+\mu^-$. Then I extend the discussion to $e^+e^- \to f\bar{f}$ where $f\bar{f}$ is any fermion-antifermion pair. In all of this lecture the interference between electromagnetic and weak processes for $e^+e^- \to f\bar{f}$ is ignored.

<u>If There Is No Z^o</u>: Let's begin by considering for comparison purposes the pure electromagnetic process

$$e^+ + e^- \to \gamma \to \mu^+ + \mu^- \qquad (4.1)$$

from Lecture 1. The diagram is Fig. 2.2a; the matrix element, Eq. (4.2), illustrates the formalism;[4.1] and Eq. (4.3) is the total cross section

$$M = \frac{e^2}{s}\,\bar{u}(2)\,\gamma^{\mu}\,u(1)\,\bar{u}(3)\,\gamma_{\mu}\,u(4) \tag{4.2}$$

where $e^2 = 4\pi\alpha$, $s = E^2_{c.m.}$, u is a Dirac spinor, and γ_{μ} is a Dirac matrix.

$$\sigma(ee \to \gamma \to \mu\mu) = 4\pi\alpha^2/3s \tag{4.3}$$

The four-fermion, point-interaction, weak process[4.1]

$$e^+ + e^- \to \mu^+ + \mu^- \quad , \quad \text{weak} \tag{4.4}$$

has the matrix element given in Eq. (4.5) in which I have generalized the usual $(1 - \gamma_5)$ term to $(v - a\gamma_5)$

$$M = \frac{G}{\sqrt{2}}\,\bar{u}(2)\,\gamma^{\mu}\,(v_e - a_e\,\gamma_5)\,u(1)\,\bar{u}(3)\,(v_{\mu} - a_{\mu}\,\gamma_5)\,u(4) \tag{4.5}$$

The total cross section and R are

$$\sigma\,(ee \to \mu\mu, \text{weak}) = \frac{G^2 s}{96\pi}\left[v_e^2 + a_e^2\right]\left[v_{\mu}^2 + a_{\mu}^2\right] \tag{4.6}$$

$$R\,(ee \to \mu\mu, \text{weak}) = \frac{G^2 s^2}{128\pi^2\alpha^2}\left[v_e^2 + a_e^2\right]\left[v_{\mu}^2 + a_{\mu}^2\right] \tag{4.7}$$

In Eqs. (4.5)-(4.7) v and a are constants which we will identify later using the Weinberg-Salam model. As $E_{c.m.}$ increases the total cross section, Eq. (4.6), eventually violates the unitarity condition $\sigma \leq \text{constant}/s$. Therefore this old theory is wrong at very high energy. Nevertheless it is interesting to compute that it gives

$$R(ee \to \mu\mu, \text{weak}) = 1 \tag{4.8}$$

at $E_{c.m.} = 150$ GeV, if we set $\left[v_e^2 + a_e^2\right]\left[v_{\mu}^2 + a_{\mu}^2\right] = 1$

<u>If There Is a Z^o</u>: If there is a Z^o of mass M_Z and width Γ_Z the reaction, Fig. 2.2b,

$$e^+ + e^- \to Z^o \to \mu^+ + \mu^- \tag{4.9}$$

has the matrix element[4.2]

$$M = \frac{GM_Z^2}{\sqrt{2}}\left[\frac{1}{s - M_Z^2 + i\Gamma_Z M_Z}\right]\bar{u}(2)\gamma^\mu(v_e - a_e\gamma_5)u(1)\bar{u}(3)\gamma_\mu(v_\mu - a_\mu\gamma_5)u(4) \tag{4.10}$$

Notice that the propagator term in the square brackets in Eq. (4.10) replaces the 1/s term in Eq. (4.2). Then

$$\sigma(ee \to Z^o \to \mu\mu) = \frac{G^2 s}{96\pi}\left[\frac{M_Z^4}{(s - M_Z^2)^2 + \Gamma_Z^2 M_Z^2}\right]\left[v_e^2 + a_e^2\right]\left[v_\mu^2 + a_\mu^2\right] \tag{4.11}$$

$$R(ee \to Z^o \to \mu\mu) = \frac{G^2 s^2}{128\pi^2\alpha^2}\left[\frac{M_Z^4}{(s - M_Z^2)^2 + \Gamma_Z^2 M_Z^2}\right]\left[v_e^2 + a_e^2\right]\left[v_\mu^2 + a_\mu^2\right] \tag{4.12}$$

In the last two equations, the square bracket term is the relativistic Breit-Wigner expression. These formula hold for the production of any elementary fermion-antifermion pair, $f\bar{f}$, via

$$e^+ + e^- \to Z^o \to f + \bar{f} \tag{4.13}$$

For later convenience I'll use

$$C_f = \left[v_e^2 + a_e^2\right]\left[v_f^2 + a_f^2\right] \tag{4.14}$$

Let's consider in turn the three $E_{c.m.}$ region

$$E_{c.m.} \ll M_Z \quad , \quad \text{far below the } Z^o$$

$$E_{c.m.} \approx M_Z \quad , \quad \text{at the } Z^o$$

$$E_{c.m.} \gg M_Z \quad , \quad \text{far above the } Z^o$$

and use the conventional values (see Eq. (4.26))

$$M_Z = 90 \text{ GeV} \quad , \quad \Gamma_Z = 2.5 \text{ GeV} \tag{4.15}$$

$\underline{E_{c.m.} \ll M_Z}$: Here

$$R(ee \to Z^o \to f\bar{f}) = \frac{G^2 s^2 C_f}{128\pi^2 \alpha^2} \tag{4.16}$$

and this is the old Fermi theory prediction, Eq. (4.7), which we have already described.

4B: At the Z^o

$\underline{e^+e^- \to Z^o \to f\bar{f}}$: At energies near the Z^o the cross section is dominated by the Breit-Wigner term in

$$\sigma(ee \to Z^o \to f\bar{f}) = \frac{G^2 s}{96\pi} \frac{M_Z^4 C_f}{(s - M_Z^2)^2 + \Gamma_Z^2 M_Z^2} \tag{4.17a}$$

$$C_f = \left[v_e^2 + a_e^2\right]\left[v_f^2 + a_f^2\right] \tag{4.17b}$$

Threshold effects, interference effects, and radiative corrections are ignored. At the peak

$$\begin{aligned} R(ee \to Z^o \to f\bar{f},\ E_{c.m.} = M_Z) &= \frac{G^2 M_Z^6 C_f}{128\pi^2 \alpha^2 \Gamma_Z^2} \\ &= 130\ C_f. \end{aligned} \tag{4.18}$$

Since C_f is about 1, R is enormous at the Z^o compared to the R values considered in the first two lectures. For example even a moderate luminosity of $10^{30}\ cm^{-2}\ sec^{-1}$ yields

$$(130)\left(\frac{.87 \times 10^{-31}}{(90)^2}\right) cm^2 \times (.36 \times 10^{34}\ cm^{-2}\ hr^{-1}) = 55\ f\bar{f}\ \text{pairs/hour} \tag{4.19}$$

Equation (4.17) applies to all the known elementary fermion pairs:[4.3-4.5]

$$\begin{aligned} &\text{charged leptons: } e^+e^-,\ \mu^+\mu^-,\ T^+T^- \quad , \\ &\text{neutrinos: } \nu_e\bar{\nu}_e,\ \nu_\mu\bar{\nu}_\mu,\ \nu_T\bar{\nu}_T \quad , \\ &\text{up class quarks: } u\bar{u},\ c\bar{c} \quad , \\ &\text{down class quarks: } d\bar{d},\ s\bar{s},\ b\bar{b} \quad ; \end{aligned} \tag{4.20}$$

and it applies to all undiscovered Fermions[4.3-4.5] which are elementary, which have conventional coupling to the Z^o, and which have mass $<(Z^o \text{ mass})/2$. Incidently if the f mass is close to $(Z^o \text{ mass})/2$, Eq. 4.17 has an additional threshold factor.

In particular the Z^o is the best way to search for neutral heavy leptons;

$$e^+ + e^- \to Z^o \to \ell^o + \bar{\ell}^o \tag{4.21}$$

will yield 5 $L^o\bar{L}^o$ pairs per hour at a luminosity of 10^{30} cm^{-2} sec^{-1} (Eq. (4.19).

$e^+e^- \to Z^o \to$ all: The total cross section and total R at the Z^o are derived from Eqs. (4.17) and (4.18) by summing over all elementary $f\bar{f}$ pairs of sufficiently small mass. I assume there are no non-fermion elementary particles with mass $<(Z^o \text{ mass})/2$ which couple to the Z^o

$$\sigma(ee \to Z^o \to \text{all}, E_{c.m.} = M_Z) = \frac{G^2 M_Z^4 C_{all}}{96\pi \Gamma_Z^2} \tag{4.22a}$$

$$R(ee \to Z^o \to \text{all}, E_{c.m.} = M_Z) = \frac{G^2 M_Z^6 C_{all}}{128\pi^2 \alpha^2 \Gamma_Z^2} \tag{4.22b}$$

$$C_{all} = [v_e^2 + a_e^2] \sum_f [v_f^2 + a_f^2] \tag{4.22c}$$

It is convenient at this point to recall the Weinberg-Salam values[4.2] of v_f and a_f, Table 4.1; and to note that all these parameters are of order 1.

Table 4.1. Weinberg-Salam model expressions for v_f, a_f; and $(v_f^2 + a_f^2)$ numerical values for $\sin^2\theta_W = 0.2$

		v_f	a_f	$v_f^2 + a_f^2$
lepton type	neutrino	+1	-1	2.00
	ℓ^-	$-1 + 4\sin^2\theta_W$	+1	1.04
quark type	up class (u,c)	$+1 - \frac{8}{3}\sin^2\theta_W$	+1	1.22
	down class (d,s,b)	$-1 + \frac{4}{3}\sin^2\theta_W$	-1	1.54

To calculate C_{all} based on the Weinberg-Salam model, the sum in Eq. (4.22c) is carried out over the 3 neutrinos, 3 charged leptons, and 5 known quarks each with three colors. Hence the minimum value of C_{all} is

$$C_{all} \geq 30 \tag{4.23}$$

Thus at the Z^o

$$R(ee \to Z^o \to \text{all}, E_{c.m.} = M_Z) \gtrsim 3700 \tag{4.24}$$

Ignoring radiative corrections and using Eq. (4.18). This is an enormous R compared to the expected one-photon-exchange R of about 5. Of course R will be larger if there are fermion or non-fermion elementary particles which couple to the Z^o and which were not counted in computing Eq. (4.23). Examples are the top quark, an ℓ^o lepton, or an elementary boson.

Searching for New Elementary Particles at the Z^o: This brings us to the question of using the Z^o to search for new elementary particles. Consider three methods:

(a) The new particles may be looked for directly by using their static and decay properties. Such searches are feasible because even a moderate luminosity gives several events per hour, Eq. (4.19).

(b) A direct measurement of R_{max} at $E_{c.m.} = M_Z$ in principle yields C_{all}; and if $C_{all} > 30$ (Eq. (4.23)), unknown particle pairs are being produced. Unfortunately this requires a few percent measurement of R_{max}. One must have very small systematic and statistical errors coming from the radiative correction, from the detector efficiency, from the luminosity measurement,

from the trigger insensitivity to $e^+e^- \to \nu\bar{\nu}$ processes, and from the effect of the spread in $E_{c.m.}$. All this seems very difficult at present.

(c) A more feasible, but still difficult, measurement is the determination of

$$\Gamma_Z = \Gamma(Z^o \to \text{all}) = \frac{GM_Z^3 C_{all}}{24\sqrt{2}\,\pi} \tag{4.25}$$

where, as before, $C_{all} = \sum_f [v_f^2 + a_f^2] \approx 30$. Then

$$\Gamma_Z \approx 2.5 \text{ GeV} \tag{4.26}$$

To find a new fermion Γ_Z must be measured to a precision much smaller than 1 part in 30. This is because a new fermion would contribute about 1 unit to C_{all}.

4.C: Beyond the Z^o

$\underline{e^+e^- \to f\bar{f}}$: When $E_{c.m.} \gg M_Z$, the propagator in Eq. (4.10) reduces to $1/s$, so that $ee \to Z^o \to f\bar{f}$ has the same s behavior as $ee \to \gamma \to f\bar{f}$. Then

$$\sigma(ee \to Z^o \to f\bar{f},\ E_{c.m.} \gg M_Z) = \frac{G^2 M_Z^4 C_f}{96\pi s} \tag{4.27}$$

$$R(ee \to Z^o \to f\bar{f},\ E_{c.m.} \gg M_Z) = \frac{G^2 M_Z^4 C_f}{128\pi^2 \alpha^2} \tag{4.28}$$

Explicitly

$$\sigma(ee \to Z^o \to f\bar{f},\ E_{c.m.} \gg M_Z) = \frac{10^{-32} C_f}{E_{c.m.}^2} \text{ cm}^2 \tag{4.29}$$

$$R(ee \to Z^o \to f\bar{f},\ E_{c.m.} \gg M_Z) = 0.11\ C_f \tag{4.30}$$

Hence for charge 1 or charge 2/3 fermions, the electromagnetic cross section is larger than the weak cross section. (I remind the reader that the interference between these two interactions has been ignored here.)

Unfortunately the neutral fermion cross section, and particularly neutral heavy lepton production, still depends on the weak process. As an example let's calculate the luminosity required to produce 1 $\ell^o\bar{\ell}^o$ pair per day at $E_{c.m.} = 1000$ GeV! Then

$$1 \text{ pair/day} = [\mathscr{L}\, \text{cm}^{-2}\, \text{sec}^{-1}][10^{-32}\, \text{cm}^2/(10^3)^2][10^5\, \text{sec/day}] \tag{4.31}$$

Hence

$$\mathscr{L} = 10^{33}\, \text{cm}^{-2}\, \text{sec}^{-1} \tag{4.32}$$

is required.

$\underline{e^+e^- \to W^+W^-,\ e^+e^- \to Z^o\bar{Z}^o}$: When $E_{c.m.} \gg M_Z$, the very important processes

$$\begin{aligned} e^+ + e^- &\to W^+ + W^- \\ e^+ + e^- &\to Z^o + \bar{Z}^o \end{aligned} \tag{4.33}$$

can be studied. If only Z^o exchange, Fig. 4.1a, contributed to these reactions; the spin 1 nature of the W and Z^o would lead to a cross section which violates unitarity as s increases. Therefore there must be additional diagrams, Figs. 4.1b and 4.1c, which cancel the unwanted s dependence. Conventional weak interaction theory naturally contains these diagrams. Hence the measurement of reactions (4.33) serves two purposes: weak interaction theory is tested, and the $W^\pm$ can be studied in some detail. Figure 4.2 gives the expected W^+W^- cross section. Notice that this is larger than the $f\bar{f}$ cross section at $E_{c.m.} = 300$ GeV. From Eq. (4.29), $\sigma(ee \to Z^o \to f\bar{f},\ E_{c.m.} = 300\ \text{GeV}) = 10^{-37}\, \text{cm}^2$.

One speculation before I turn to the final subject: e^+e^- machines at very high energy. This discussion of the $E_{c.m.} \gg M_Z$ region has been based on the assumption that there is just one Z^o with a mass of about 90 GeV. However, if there were a sequence

$$Z^o,\ Z^{o'},\ Z^{o''}\ \ldots$$

with increasing masses, the very useful R enhancement which occurs at the Z^o, Eq. (4.18), would occur again at higher energies.

4D: Very High Energy e^+e^- Colliding Beams Machines

The Synchrotron Radiation Problem in e^+e^- Storage Rings: All existing e^+e^- machines are of the storage ring type described in Sec. 1A. As the $E_{c.m.}$ of such machines increases, there is a very rapid increase in the power lost by the electrons and positrons through synchrotron radiation.[4.6] [Synchrotron radiation is the electromagnetic radiation emitted by a charged particle moving through a curved path.] Explicitly the radio frequency voltage required per turn to replace the lost energy is

$$V_{rf} = \text{constant}\ (E_b^4/\rho) \tag{4.34}$$

where ρ is the radius of bending and E_b is the beam energy. The power required is

$$P_{in} = (V_{rf}\, I + V_{rf}^2/R)/\varepsilon \tag{4.35}$$

where ε is the efficiency of converting 60 cycle power to rf power, I is the total current in the e^- and e^+ beams, and the second term is the resistive power loss in the rf cavities. Superconducting cavities can eliminate this second term; however, the power required for refrigeration and increased construction costs may approximately cancel the reduction in rf power costs.

Equations (4.34) and (4.35) and other considerations have led e^+e^- storage ring designers[4.7,4.8] to the rough rule that the optimum design requires

$$R \propto E_b^2 \tag{4.36a}$$

Since construction costs scale as the circumference of the ring

$$\text{construction costs} \propto R \propto E_b^2 \tag{4.36b}$$

LEP: CERN is proposing to build a very large e^+e^- storage ring called LEP.[4.9] I shall describe this proposed machine briefly because of the powerful e^+e^- physics it can do, and because it appears to yield the highest energies attainable in conventionally designed and economically feasible e^+e^- storage rings.

LEP will have a circumference of about 31 km. It is designed to have eight interaction regions but will probably start with four. The RF power will be installed in stages as outlined in Table 4.2. Stage 1/6 will allow the Z^o to be produced if its mass is less than 100 GeV. Stage 2 assumes the room temperature, copper, rf cavities are replaced by superconducting cavities. If superconducting cavities are not available, additional copper cavities could be added to give stage 4/3.

The total construction cost of this machine will be about 10^9\$. The power cost at stage 1/6 will be about

$$(9 \times 10^4 \text{ kW})(6 \times 10^3 \text{ hrs/yr})(0.1 \text{ \$/kW hr}) = 5 \times 10^7 \text{ \$/yr}$$

Stage 1 will have about 2.5 times the power cost. These costs are very well justified by the tremendous range of e^+e^- physics which will be done by this facility. However Eq. (4.36b) makes it clear that it is not economically feasible to obtain a factor of 2 or 3 increase in $E_{c.m.}$ using this type of storage ring.

Table 4.2. Proposed stages in the addition of RF power to LEP. From Ref. 4.9

Stage	1/6	1/3	1	4/3	2
$E_{c.m.}$ (GeV)	~100.	~125.	~170.	~185.	~260.
Luminosity (10^{32} cm^{-2} sec^{-1})	0.4	0.6	1.1	1.2	1.0
Current (mA)	6.	7.	9.	9.	6.
RF power used (MW)	16.	32.	96.	128.	96.
Total power (MW)	90.	128.	254.	317.	

e^+e^- Colliding Linear Accelerators: An alternative to an e^+e^- colliding beams storage ring is the colliding of the e^+ and e^- beams from a pair of linear accelerators, Fig. 4.3. A general review of colliding linear accelerator ideas and theory has been given by Amaldi.[4.10] He also gives a full set of references to the contributors to the field and its history. A brief review has been given by Richter.[4.8] I will present a very brief comparison of the two types of e^+e^- colliding beams machines.

In a storage ring, Sec. 1A, the total luminosity is

$$\mathscr{L}_{ring} = \frac{n_{IR} n_b N_{ring}^2 f_{ring}}{A_{ring}} \tag{4.37}$$

Here n_{IR} is the number of interaction regions; n_b is the number of e^+ or e^- bunches; N_{ring} is the number of e^+ or e^- in a bunch; A_{ring} is the cross sectional area of a bunch, and f_{ring} is the bunch rotation frequency.

In a colliding (also called clashing) linear accelerator facility

$$\mathscr{L}_{linac} = \frac{n_b N_{linac}^2 f_{linac}}{A_{linac}}$$

Here f_{linac} is the linear accelerator pulse rate, and each pair of bunches is assumed to collide just once. The length L is proportional to E_b and the construction cost is proportional to L; hence:

$$\text{Construction cost} \propto L \propto E_b \quad . \tag{4.38}$$

Figure 4.4 shows a qualitative comparison of the construction costs of storage rings and clashing linacs. At present we do not know where the crossover occurs; knowing enough to calculate the crossover point is one of the major objects in developing colliding linac technology.

Luminosity Comparison: To give a general idea of the requirements on a colliding linac I will make a crude comparison with an $E_{c.m.} = 200$ GeV LEP type storage ring. For such a storage ring N_{ring} is 5×10^{11} to 10^{12} particles per bunch; we will use

$$\begin{aligned} N_{ring} &\sim 10^{12} \text{ particles/bunch} \\ A_{ring} &\sim 4\pi \times 100\mu \times 30\mu \sim 10^4 \pi\mu^2; \ (\mu = \text{micron}) \\ f_{ring} &\sim \frac{3 \times 10^8 \text{ m/sec}}{30 \times 10^3 \text{ m}} = 10^4 \text{ Hz} \\ n_b &\sim 4 \text{ bunches}; \ n_{IR} = 4 \quad . \end{aligned} \tag{4.39}$$

In a linear accelerator purposely built for a clashing linac we expect

$$\begin{aligned} N_{linac} &\sim 10^{11} \text{ particles/bunch} \\ f_{linac} &\sim 10^3 \text{ Hz} \\ n_b &\sim 2 \text{ bunches} \quad . \end{aligned} \tag{4.40}$$

Then from Eqs. (4.39) and (4.40)

$$\frac{\mathscr{L}_{linac}}{\mathscr{L}_{ring,\,IR}} \approx \left(\frac{10^{11}}{10^{12}}\right)^2 \left(\frac{2 \times 10^3}{16 \times 10^4}\right) \left(\frac{A^{ring}}{A_{linac}}\right) \approx 10^{-4} \left(\frac{A^{ring}}{A_{linac}}\right)$$

For the same $\mathscr{L}$

$$A_{linac} \approx 10^{-4} \, A_{ring} \approx \pi \text{ micron}^2$$

If the linac beam has a circular cross section of radius r_{linac}

$$r_{linac} \approx 1 \text{ micron} \tag{4.41}$$

Equation (4.41) states the crucial requirement on e^+e^- clashing linac technology to obtain a luminosity equal to the total luminosity of an

e^+e^- storage ring. We must learn to make, accelerate, steer, focus and collide e^- and e^+ bunches with 10^{11} particles per bunch and with one micron transverse dimensions at the collision point. Studies now in progress indicate that this can be done.

The SLAC Linear Collider: B. Richter has proposed a very ingenious application of the clashing linacs principle to the existing SLAC linear accelerator. This proposal,[4.5] shown schematically in Fig. 4.5, contains the following elements:

(a) Using the SLED mode[4.11] of operation of the accelerator the accelerator energy is raised to about 50 GeV.

(b) The e^- bunch and the e^+ bunch are accelerated in the same accelerator pulse, one bunch following the other one down the accelerator separated by a distance of the order of tens of meters.

(c) The e^- and e^+ bunches are transported in opposite directions by the roughly circular transport system to the interaction point.

(d) At the interaction point the bunches, which were of the order of 100 μ in transverse dimensions as they left the linac, are focused by the transport system and interaction regions quadrupoles to transverse dimensions of the order of several microns.

The initial parameters of the proposed facility are:

$$E_{c.m.} \approx 2 \times 50 \text{ GeV} \approx 100 \text{ GeV}$$

$$N \approx 5 \times 10^{10} \text{ particles/bunch}$$

$$f = 180 \text{ Hz}$$

$$\sigma_r \approx 2\mu$$

$$\mathscr{L} = \frac{N^2 f}{4\pi \sigma_r^2} \approx 10^{30} \text{ cm}^{-2} \text{ sec}^{-1}$$

Here σ_r is the root mean square transverse radius of the bunches. The length of the bunches will be several mm. By further SLED type improvements, the addition of more klystrons to the linear accelerator, and other improvements, it is possible in principle to increase the $E_{c.m.}$ to about 130 or 140 GeV.

The luminosity can probably be increased to

$$\mathscr{L}_{max} \approx 10^{31} \text{ cm}^{-2} \text{ sec}^{-1}$$

by increasing N by a factor of 2, by decreasing σ_r^2 by a factor of 2, and by using the focusing effect that each beam has on the other.[4.12]

The Future of e^+e^- Physics: Thus e^+e^- physics has a bright future. A new set of high energy e^+e^- storage rings--CESR, PEP, PETRA--has just gone into operation. Older storage rings--DCI, DORIS, SPEAR, VEPP-2M, and VEPP-4--continue to do very interesting physics. We now have proposals for a new low energy storage ring, ALA; and for very high energy storage rings, LEP and HERA. And a new technology, colliding linear accelerators, is being developed which can take us to yet higher energies.

Acknowledgement: I am very grateful to Professors Hanu Miettinen and Matts Roos of the University of Helsinki for having encouraged me to give these lectures. I want to thank the organizers and staff of the Arctic School of Physics for having conducted an extremely useful and productive summer school.

References for Lecture 1

1.1 The most comprehensive general reference for e^+e^- storage ring theory is M. Sands, The Physics of Electron Storage Rings, SLAC Report SLAC-121 (1970). This and other storage ring articles are contained in Physics With Intersecting Storage Rings, (Academic Press, New York, 1970), ed. by B. Touschek. See also C. Pellegrini, Ann. Rev. Nucl. Sci. 22, 1 (1972). For brief descriptions of some recent e^+e^- storage rings see: B. D. McDaniel, IEEE Trans. Nucl. Sci. NS-26, 2978 (1979); G. A. Voss et al., IEEE Trans. Nucl. Sci. NS-26, 2970 (1979).

1.2 Some references to very high energy e^+e^- storage rings are: B. Richter, Nucl. Inst. Meth. 136, 47 (1976); E. Keil, Proc. of 1979 Int. Sym. on Lepton and Photon Int. at High Energies (Fermi Nat. Lab., Batavia, 1979), p. 305; and Proc. Second ICFA Workshop on Possibilities and Limitations of Accelerators and Detectors (CERN, Les Diablerets, 1979), ed. by U. Amaldi.

1.3 R. F. Schwitters and K. Strauch, Ann. Rev. Nucl. Sci. 26, 89 (1976).

1.4 The highest energy tests of QED in e^+e^- annihilation come from experiments at the PETRA e^+e^- stroage ring: D. P. Barber et al., Phys. Rev. Lett. 43, 1915 (1979); S. Orito, Proc. 1979 Int. Sym. on Lepton and Photon Int. at High Energy (Fermi Nat. Lab., Batavia, 1979), p. 52; C. Berger et al., Zeit. Phys. C4, 269 (1980); R. Brandelik et al., DESY Preprint DESY 80/33 (1980).

1.5 See for example: J. J. Sakurai, UCLA Preprint UCLA/180/TEP/14 (1980); D. P. Barber et al., Physikalische Inst. Rwth. Aachen Preprint TITHA 80/8 (1980).

1.6 J. L. Siegrist, Ph.D. Thesis, SLAC Report SLAC-225 (1980).

1.7 Two reviews of the data for $e^+e^- \to$ hadrons at high energy are: G. Wolf, DESY Preprint DESY 80/13 (1980); and G. Flügge, Kernforschungszentrum Karlsruhe Preprint KfK 2995 (1980).

1.8 R. Brandelik et al., Z. Phys. C4, 87 (1980).

1.9 For an interesting discussion of the application of QCD to R see R. M. Barnett, M. Dine, and L. McLerran, SLAC Preprint SLAC-PUB-2475 (1980), submitted to Phys. Rev.

References for Lecture 2

2.1 The following references provide an introduction to the concept of composite leptons: H. Harari, Phys. Lett. 86B, 83 (1979); G. L. Shaw, Phys. Lett. 81B, 343 (1979); S. J. Brodsky and S. D. Drell, SLAC Preprint SLAC-PUB-2534 (1980), submitted to Phys. Rev.

2.2 For early references see: M. L. Perl and P. Rapidis, SLAC Preprint SLAC-PUB-1496 (1974), unpublished; C. H. Llewellyn Smith, Proceedings of the Royal Society (London) A355, 585 (1977).

2.3 The history of the discovery of the tau is given in: M. L. Perl, Nature 275, 273 (1978); see also Ya. I. Azimov, L. L. Frankfurt, and V. A. Khoze, Sov. Phys. JETP 45, 32 (1977).

2.4 M. L. Perl, Ann. Rev. Nucl. Part. Sci. 30, 299 (1980).

2.5 Y. S. Tsai, Phys. Rev. D4, 2821 (1971); H. B. Thacker and J. J. Sakurai, Phys. Lett. 36B, 103 (1971).

2.6 See for example: J. D. Bjorken and S. D. Drell, Relativistic Quantum Mechanics, (McGraw Hill, New York, 1964); J. J. Sakurai, Advanced Quantum Mechanics (Addison-Wesley, Reading, 1967).

2.7 R. Brandelik et al., Phys. Lett. 92B, 199 (1980).

2.8 J. D. Bjorken and C. H. Llewellyn Smith, Phys. Rev. D7, 88 (1973).

2.9 S. P. Rosen, Phys. Rev. Lett. 40, 1057 (1978).

2.10 See for example: G. R. Farrar and P. Fayet, Phys. Lett. 89B, 191 (1980); G. Barbiellini et al., DESY preprint DESY 79/67 (1979) entitled, "Supersymmetric Particles at LEP."

2.11 J. Leite Lopes, J. A. Martins Simoes, and D. Spehler, Université Louis Pasteur Preprint CRN/HE 80-8 (1980).

2.12 For lepton production in hadron-hadron collisions see: R. Bhattacharya, J. Smith and A. Soni, Phys. Rev. D13, 2150 (1976); G. Chu and J. F. Gunion, Phys. Rev. D11, 73 (1975).

2.13 Examples of recent searches using Fermilab are: S. Frankel et al., Phys. Rev. 12D, 2561 (1975); J. W. Cronin et al., Phys. Rev. 10D, 3093 (1974).

2.14 Y. S. Tsai, Rev. Mod. Phys. 46, 815 (1974).

2.15 J. Smith. A. Soni and J.A.M. Vermaseren, Phys. Rev. D15, 648 (1977).

2.16 See for example A. M. Cnops et al., Phys. Rev. Lett. 40, 144 (1978).

2.17 M. L. Perl in Proc. Topical Workshop on Production New Particles in Super High Eerngy Collisions, (Univ. of Wisc. Madison, 1979), ed. by V. Barger and F. Halzen.

2.18 A. Zichichi et al., INFN/AE-67/3 (1967).

2.19 M. Bernardini et al., Nuovo Cimento 17, 383 (1973).

2.20 S. Orito et al., Phys. Lett. 14, 238 (1974).

2.21 G. Wolf, Proc. 1980, SLAC Summer Inst. Particle Phys., to be published as SLAC Report.

2.22 W. Bartel and O. A. Petersen, DESY Preprint DESY 80/46 (1980).

2.23 W. Bartel et al., DESY Preprint DESY 80/71 (1980).

2.24 H. Spitzer, DESY Preprint DESY 80/46 (1980).

2.25 K. Hayes, Stanford Univ. Ph.D. Thesis (1980), unpublished (to be published as Phys. Rev. article).

2.26 Many searches for e^* and μ^* leptons were carried out at ADONE; see for example: M. Bernardini, Proc. Int. Sym. Electron and Photon Interactions at High Energies, 1971 (Lab. for Nucl. Sci., Cornell, 1971); C. Bacci et al., Phys. Lett. 44B, 530 (1973); also M. L. Perl and P. Rapidis in Ref. 2.2 compare e^+e^- searches with other search methods.

2.27 G. Flügge, Zeit. Phys. C1, 121 (1979); G. Wolf, DESY Preprint DESY 80/13 (1980).

2.28 J. Kirkby, Proc. 1979 Int. Sym. on Lepton and Photon Interactions at High Energy (Fermi Nat. Lab., Batavia, 1979).

2.29 S. Ting, private communication and D. P. Barber et al., Phys. Rev. Lett. 43, 1915 (1979).

2.30 J. Jaros et al., Supplement B to PEP-5 Proposal to SLAC (July, 1980), unpublished.

2.31 I. Pless et al., Proposal-P636 to Fermi Nat. Lab. (April, 1980), unpublished.

2.32 C. Baltay et al., Proposal-P646 to Fermi Nat. Lab. (May, 1980).

2.33 C. A. Blocker, Ph.D. Thesis, LBL Report LBL-10801 (1980).

2.34 See for example: S. M. Bilenky and B. Pontecorvo, Phys. Reports 41, 225 (1978); V. Barger et al., Univ. of Wisconsin Preprint COO-881-148 (1980); A. DeRujula et al., CERN Preprint CERN TH-2788 (1980).

2.35 C. H. Albright and R. E. Shrock, Phys. Lett. 84B, 123 (1979).

2.36 V. Barger and R. Phillips, Phys. Lett. 74B, 393 (1978).

2.37 F. Sciulli, Proc. Neutrino-78 (Purdue Univ., West Lafayette, 1978).

2.38 These proposals, all made in 1980 to Fermi Nat. Lab. are: V. F. Kaftanov et al., P633; I. Pless et al., P636; M. Longo et al., P644; W. Lee et al., P654; and S. Whitaker et al., P656.

2.39 B. P. Roe et al., Experiment E613 at Fermi Nat. Lab.

2.40 For a review of the CERN experiments see H. Wachsmuth, Proc. 1979 Int. Sym. Lepton and Photon Interactions at High Energies (Fermi Nat. Lab, Batavia, 1979).

2.41 Current measurements give T_F in the range of 1 to 5×10^{-13} sec; see for example the summary by J. Mulvey, Proc. 1980 SLAC Summer Inst. Particle Phys., to be published as SLAC Report.

References for Lecture 3

3.1 E. Eichten et al., Phys. Rev. 17D, 3090 (1978).

3.2 J. L. Rosner, Univ. of Minnesota, Preprint 79-1015 (1979) and Univ. of Minnesota Preprint 80-0592.

3.3 C. Quigg, Proc. 1979 Int. Sym. Lepton and Photon Interactions at High Energies (Fermi Nat. Lab., Batavia, 1979).

3.4 K. Gottfried, Cornell Univ. Preprint CLNS 80/467 (1980), submitted to Comments in Nuclear and Particle Physics.

3.5 M. L. Perl, High Energy Hadron Physics (Wiley, New York, 1974).

3.6 J. -E. Augustin et al., Phys. Rev. Lett. 33, 1406 (1974).

3.7 J. J. Aubright et al., Phys. Rev. Lett. 33, 1404 (1974).

3.8 G. J. Feldman and M. L. Perl, Phys. Reports 33C, 285 (1977).

3.9 S. W. Herb et al., Phys. Rev. Lett. 39, 252 (1977); W. R. Innes et al., Phys. Rev. Lett. 39, 1240 (1977).

3.10 See for example the review of H. Meyer, Proc. 1979 Int. Sym. Lepton and Photon Interactions at High Energies (Fermi Nat. Lab., Batavia, 1979).

3.11 See for example: G. Moneti, Proc 1980 SLAC Summer Inst. on Particle Phys., to be published as a SLAC Report; K. Berkelman, Proc. XXth Int. Conf. on High Energy Physics (Univ. of Wisconsin, Madison, 1980), to be published.

3.12 N. Barash-Schmidt et al., Review of Particle Properties in Rev. Mod. Phys. 52, No. 2 (1980).

3.13 See a text on non-relativistic quantum mechanics.

3.14 J. D. Jackson, SLAC Report SLAC-198 (1976), p. 180.

3.15 A. Martin, Phys. Lett. 93B, 338 (1980).

3.16 J. L. Richardson, Phys. Lett. 82B (1979).

References for Lecture 4

4.1 J. D. Bjorken and S. D. Drell, Relativistic Quantum Mechanics (McGraw Hill, New York, 1964); J. J. Sakurai, Advanced Quantum Mechanics (Addison-Wesley, Reading, 1967).

4.2 J. Ellis in CERN preprint CERN 79-01, Vol. 1, pp. 613-636 (1979).

4.3 See for example CERN preprint CERN 76-18 (1976) entitled, "Physics with Very High Energy e^+e^- Colliding Beams."

4.4 For comprehensive discussions see: B. L. Ioffe and V. A. Khoze, Sov. J. Part. Nucl. 9, 50 (1978).

4.5 SLAC Linear Collider Design Report, SLAC-229 (1980).

4.6 See Ref. 1.1.

4.7 For a recent review of very high energy e^+e^- colliding beam storage rings see E. Keil, Proceedings of 1979 International Symposium on Lepton and Photon Physics at High Energy (Fermi National Laboratory, Batavia, Illinois, 1979).

4.8 B. Richter, IEEE Transactions on Nuclear Science NS-26, 4261 (1979).

4.9 See CERN Report CERN/ISR-LEP/79-33 (1979), entitled "Design Study of a 22-GeV to 130-GeV e^+e^- Colliding Beams Machine (LEP).

4.10 U. Amaldi, Proceedings of 1979 International Symposium on Lepton and Photon Interactions at High Energy (Fermi National Laboratory, Batavia, Illinois, 1979).

4.11 Z. D. Farkas, et al., Proceedings of IX International Conference on High Energy Accelerators (Stanford Linear Accelerator Center, Stanford, California, 1974), p. 576; G. A. Loew, Proceedings of X International Conference on High Energy Accelerators (Serpukhov, USSR, 1977), p. 58.

4.12 R. Hollebeek, SLAC Preprint SLAC-PUB-2535 (1980), to be published.

Figure Captions

1.1 (a) A single ring colliding beams machine; (b) a double ring colliding beams machine; (c) the cross section of an e^+ or e^- bunch transverse to the direction of motion of the bunch.

1.2 Plot of the design luminosities of CESR and PEP, and attained luminosity of SPEAR, from B. D. McDaniel, Ref. 1.1.

1.3 (a) Feynman diagram for $e^+e^- \to \mu^+\mu^-$; (b) possible modification to the QED prescription for $e^+e^- \to \mu^+\mu^-$; (c) an additional diagram exchanging an X particle can modify the propagator for one-photon-exchange; (d) an additional diagram which contributes to $e^+e^- \to e^+e^-$.

1.4 (a) The naive quark model for non-resonant production of hadrons in e^+e^- annihilation; (b) the resonant production of hadrons in e^+e^- annihilation.

1.5 The ratio $R = \sigma(e^+e^- \to \text{hadrons})/\sigma(e^+e^- \to \mu^+\mu^-)$ versus $E_{c.m.}$ from SPEAR, from Ref. 1.6.

1.6 The ratio $R = \sigma(e^+e^- \to \text{hadrons})/\sigma(e^+e^- \to \mu^+\mu^-)$ versus $E_{c.m.}$ showing recent PETRA data, from Ref. 1.8.

2.1 A crude method for calculating the decay branching fractions for a heavy lepton.

2.2 (a) One-photon-exchange diagram for $e^+e^- \to \ell^+\ell^-$; (b) one-Z^o-exchange diagram for $e^+e^- \to \ell^o\bar{\ell}^o$.

2.3 Schematic drawing of production of a ν_τ, $\bar{\nu}_\tau$ beam by stopping a proton beam in a target and beam dump.

3.1 (a) A resonance with the non-relativistic Breit-Wigner shape, Eq. (3.8b); (b) a resonance with the same area as that in (a), but broadened by $\Gamma_{observed} = 4\Gamma$.

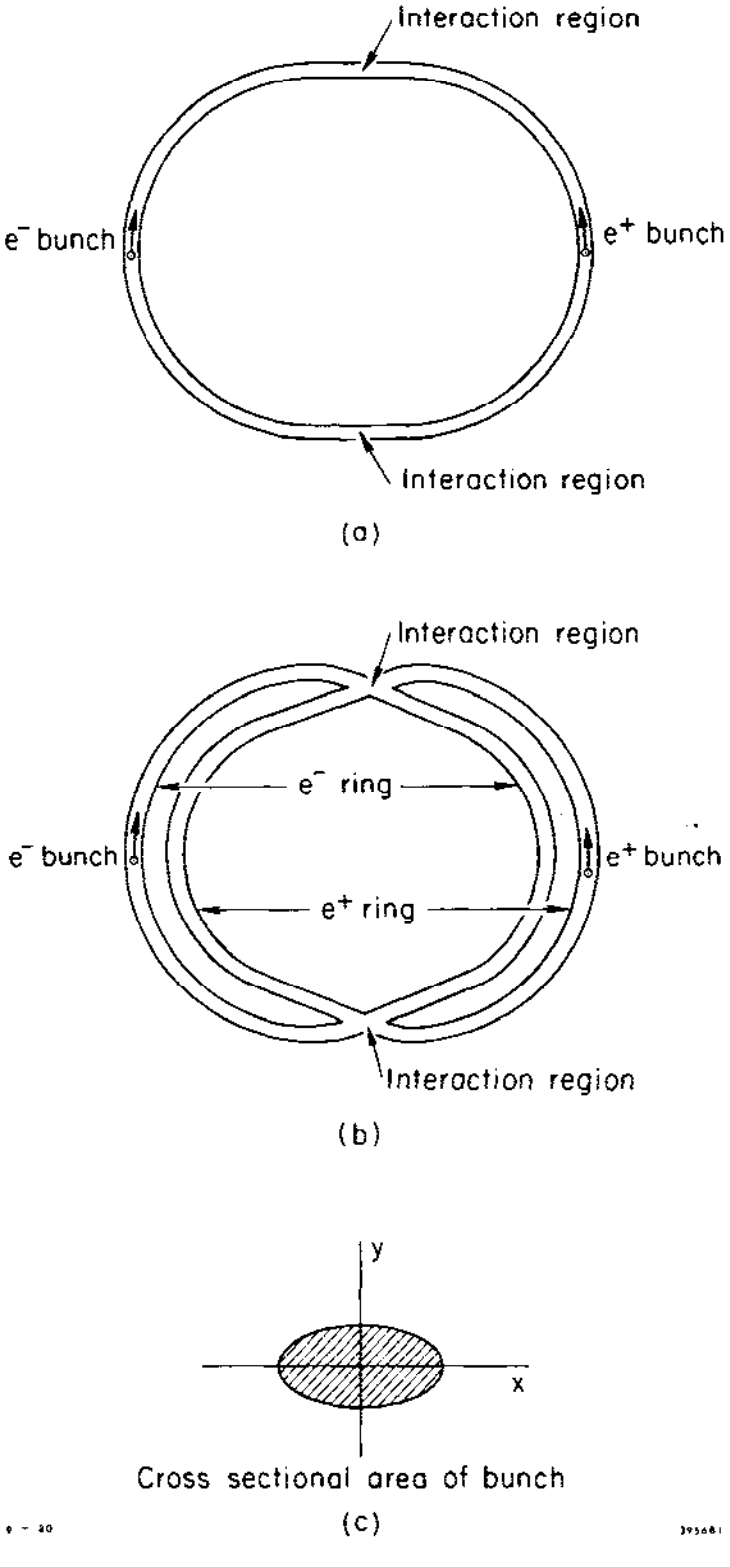
Interaction region
e⁻ bunch
e⁺ bunch
Interaction region
(a)
Interaction region
e⁻ ring
e⁻ bunch
e⁺ bunch
e⁺ ring
Interaction region
(b)
y
x
Cross sectional area of bunch
(c)

Fig. 1.1

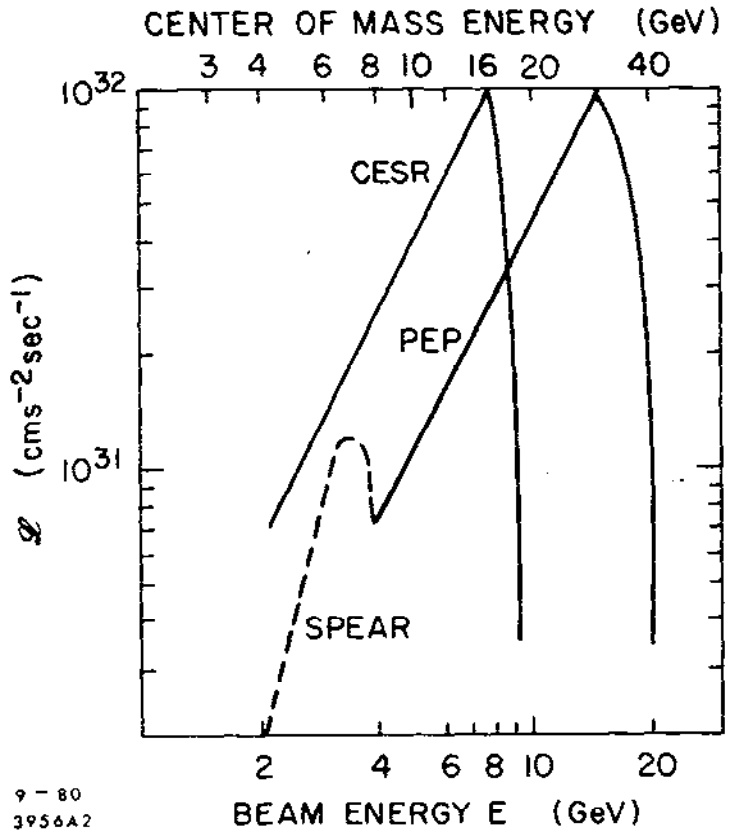
CENTER OF MASS ENERGY (GeV)
3 4 6 8 10 16 20 40
10^{32}
10^{31}
$\mathscr{L}$ ($cms^{-2}sec^{-1}$)
CESR
PEP
SPEAR
2 4 6 8 10 20
BEAM ENERGY E (GeV)
9-80
3956A2

Fig. 1.2

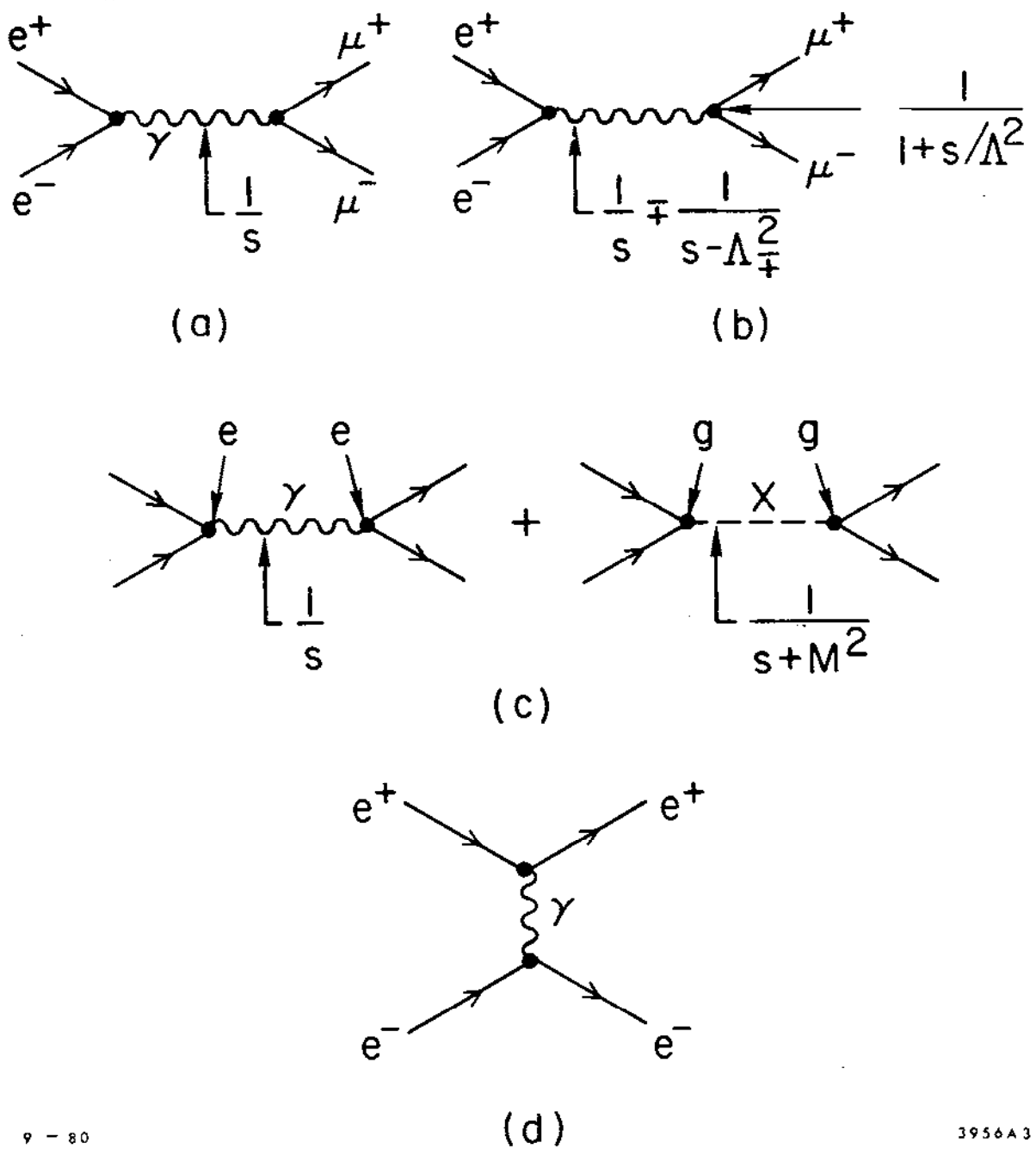
e+
μ+
γ
e−
μ−
1/s
(a)
e+
μ+
μ−
e−
1/s ∓ 1/(s−Λ±²)
1/(1+s/Λ²)
(b)
e
e
γ
1/s
+
g
g
X
1/(s+M²)
(c)
e+
e+
γ
e−
e−
(d)
9 − 80
3956A3

Fig. 1.3

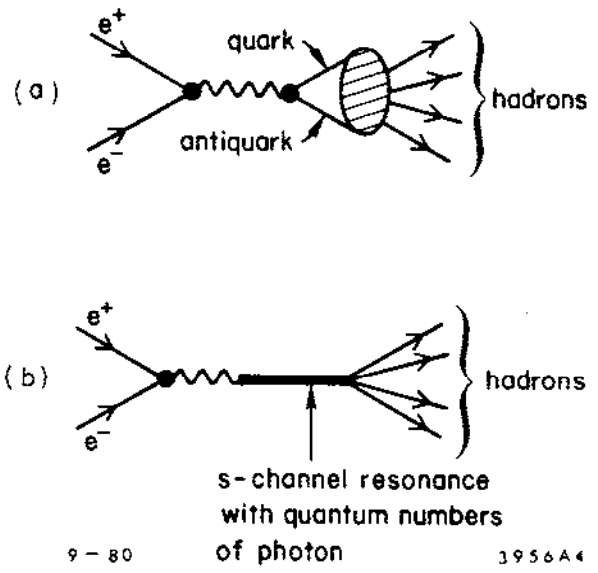
(a)
e+
e−
quark
antiquark
hadrons
(b)
e+
e−
hadrons
s-channel resonance
with quantum numbers
of photon
9-80
3956A4

Fig. 1.4

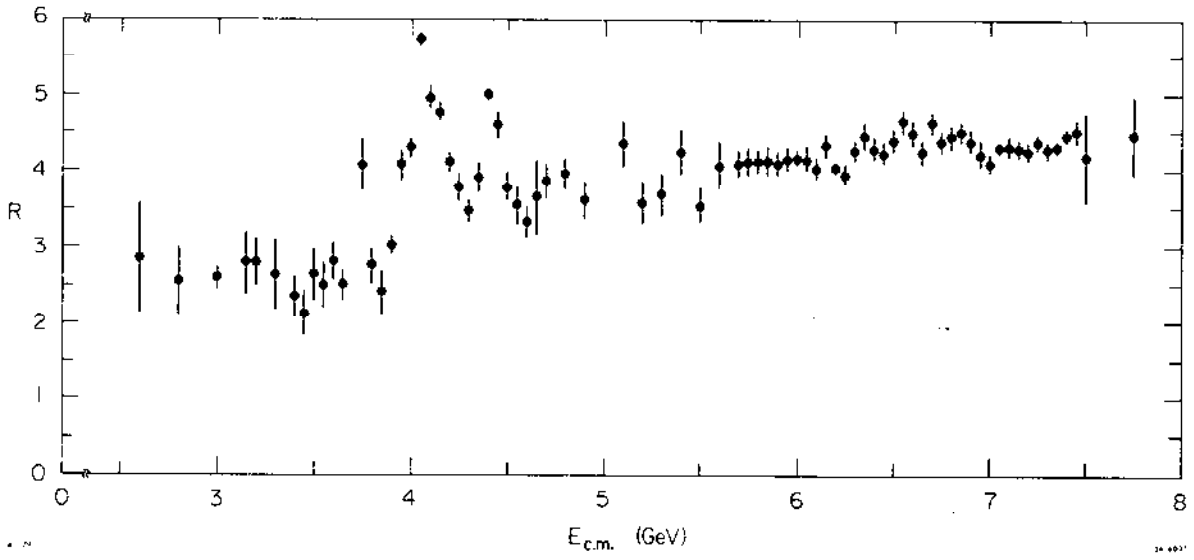

Fig. 1.5

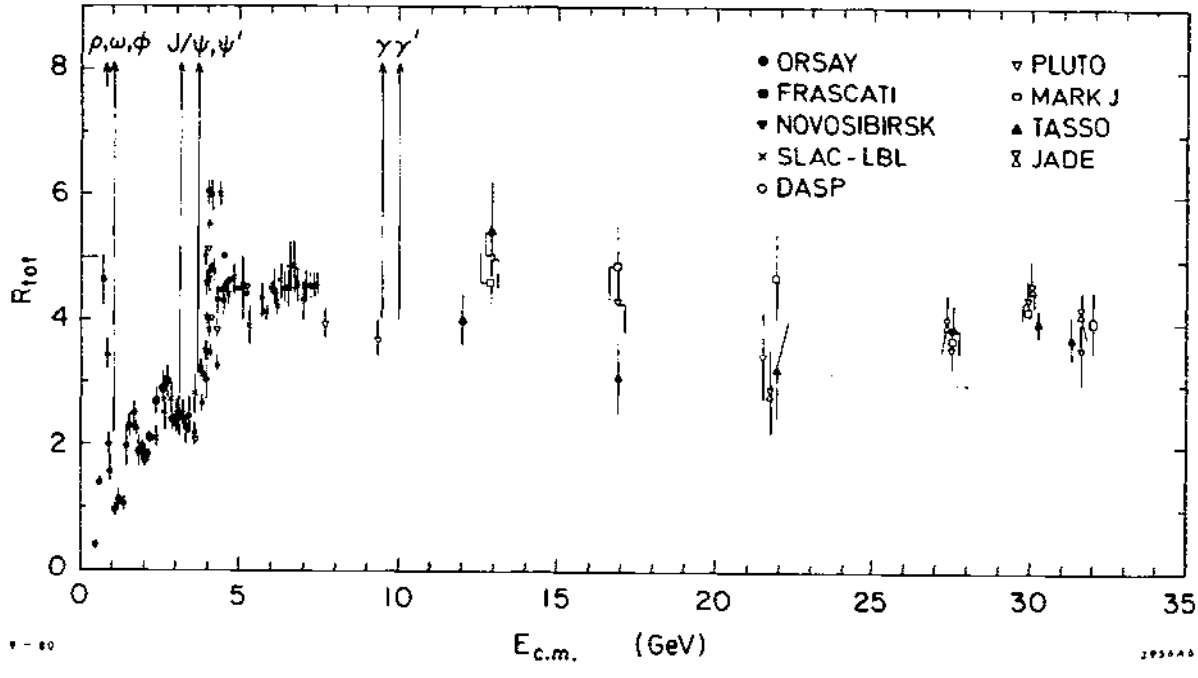
ρ,ω,φ
J/ψ,ψ'
γγ'
• ORSAY
▪ FRASCATI
▾ NOVOSIBIRSK
× SLAC - LBL
○ DASP
▽ PLUTO
○ MARK J
▲ TASSO
⧖ JADE
R_tot
E_c.m. (GeV)
0
2
4
6
8
0
5
10
15
20
25
30
35

Fig. 1.6

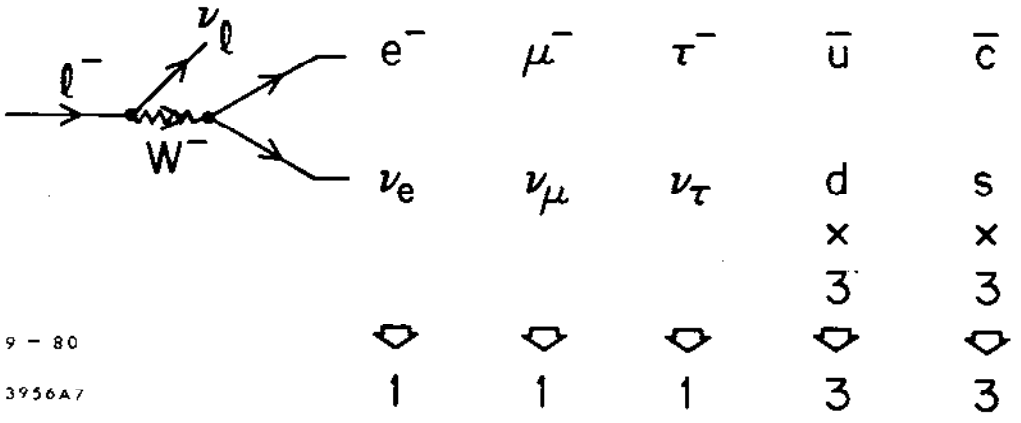
ν_ℓ
ℓ^-
W^-
e^-
μ^-
τ^-
$\bar{u}$
$\bar{c}$
ν_e
ν_μ
ν_τ
d
s
×
×
3
3
9 - 80
3956A7
1
1
1
3
3

Fig. 2.1

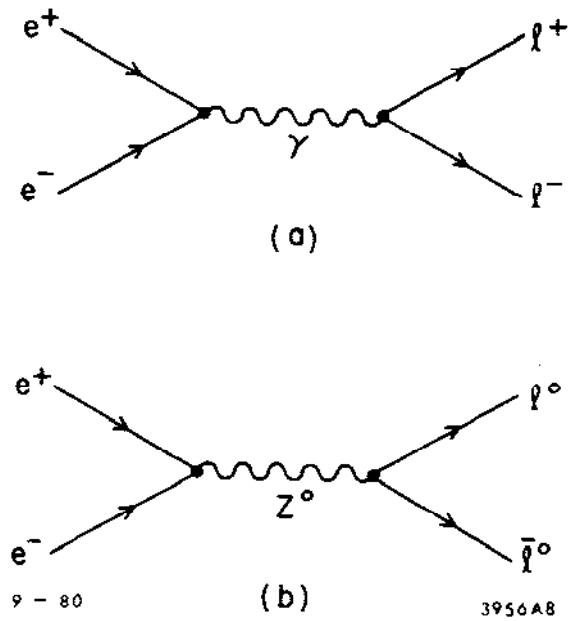

Fig. 2.2

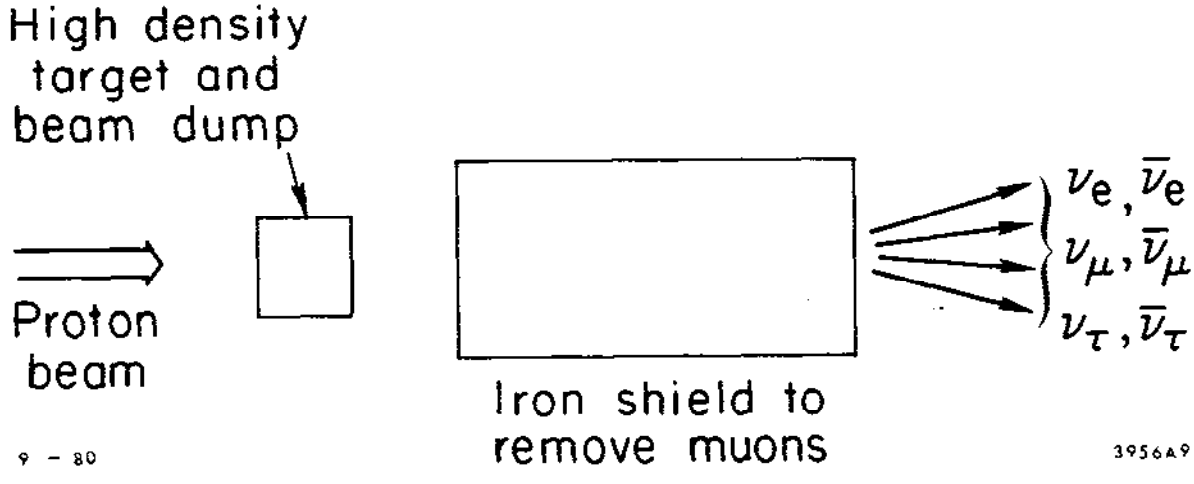
High density
target and
beam dump
Proton
beam
Iron shield to
remove muons
$\nu_e, \bar{\nu}_e$
$\nu_\mu, \bar{\nu}_\mu$
$\nu_\tau, \bar{\nu}_\tau$
9 - 80
3956A9

Fig. 2.3

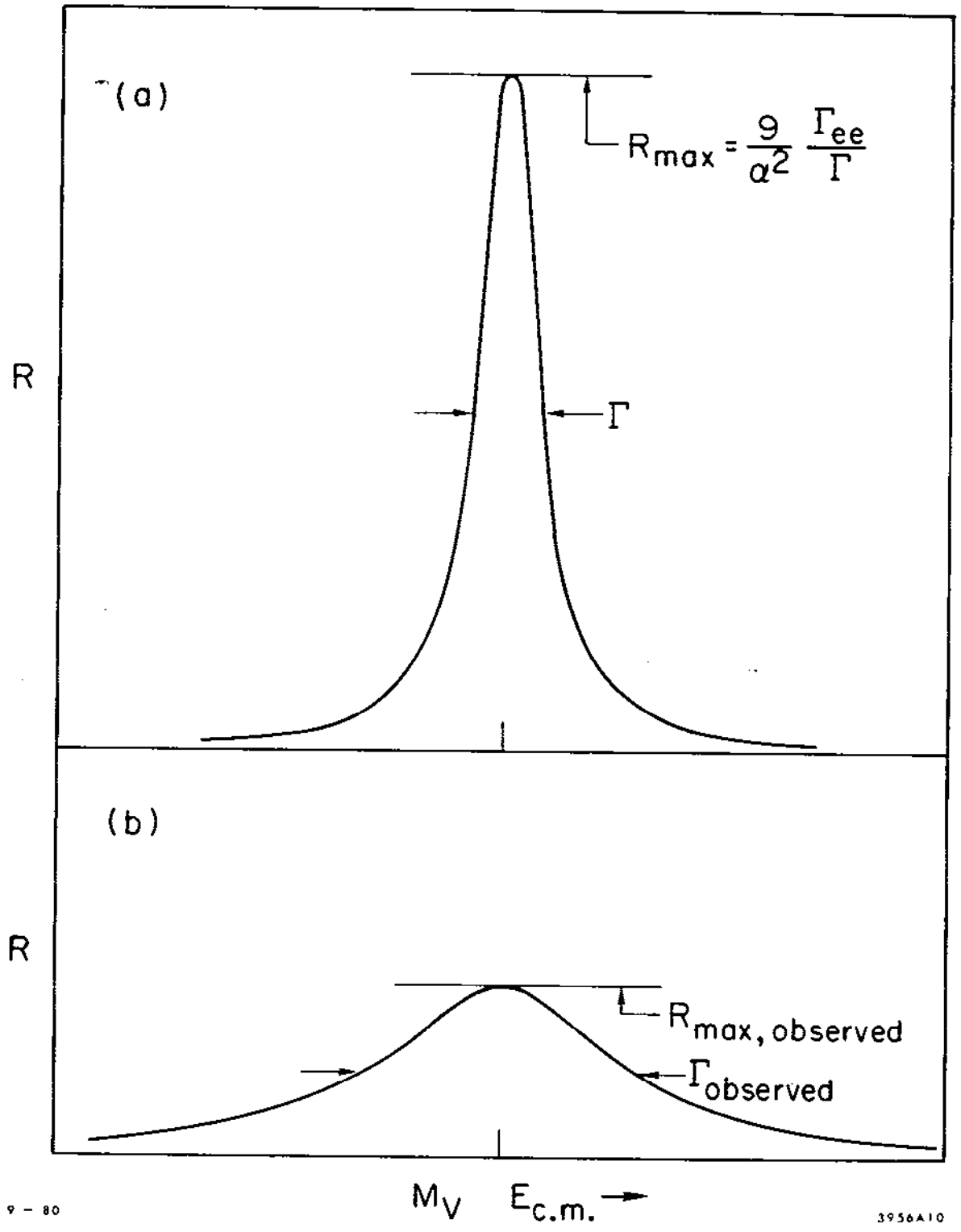
(a)
$R_{max} = \frac{9}{\alpha^2} \frac{\Gamma_{ee}}{\Gamma}$
R
Γ
(b)
R
$R_{max, observed}$
$\Gamma_{observed}$
M_V $E_{c.m.}$ →
9 - 80
3956A10

Fig. 3.1

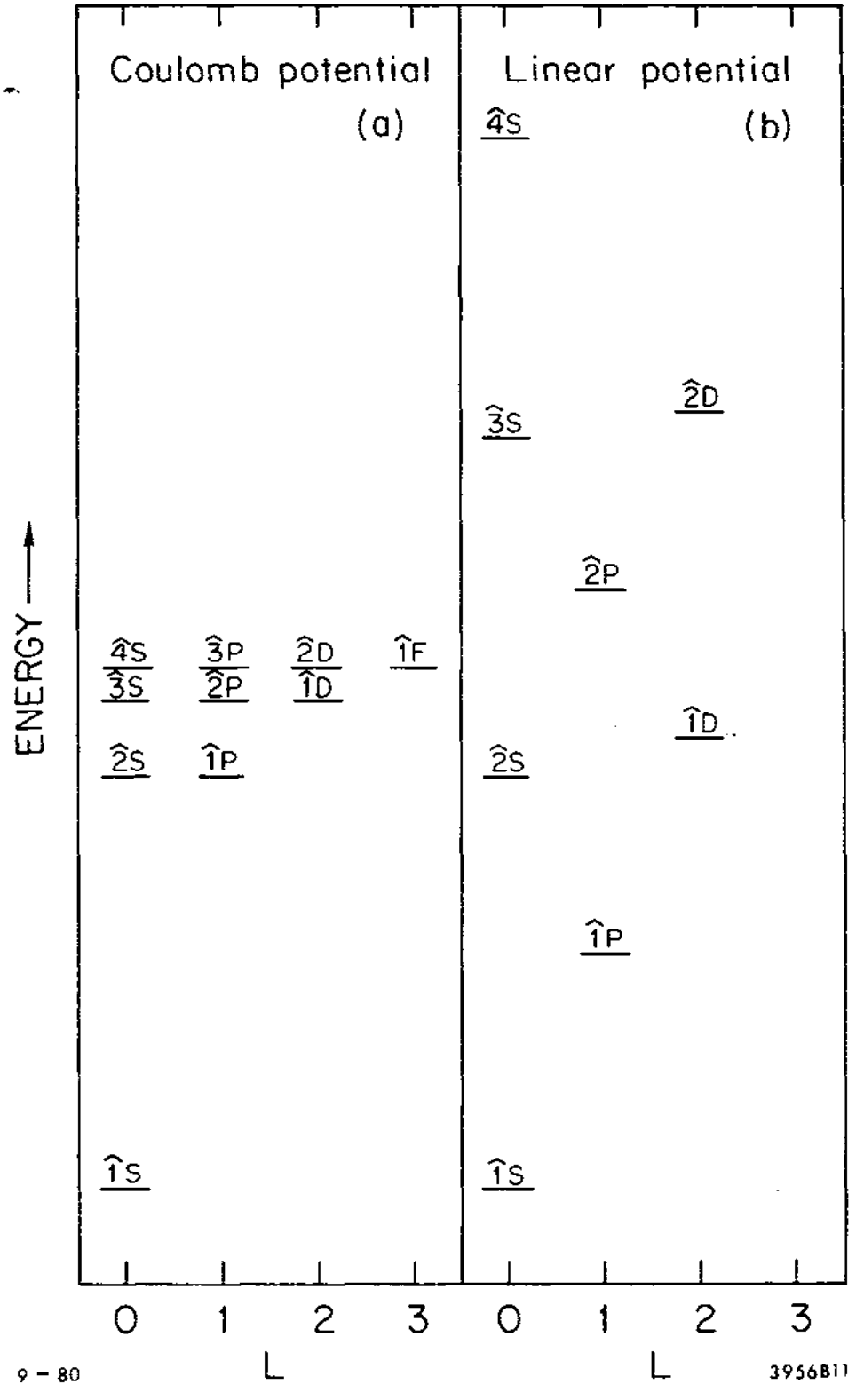
Coulomb potential
(a)
Linear potential
(b)
ENERGY
4̂S
3̂S
2̂S
1̂S
3̂P
2̂P
1̂P
2̂D
1̂D
1̂F
0
1
2
3
L
9 - 80
3956B11

Fig. 3.2

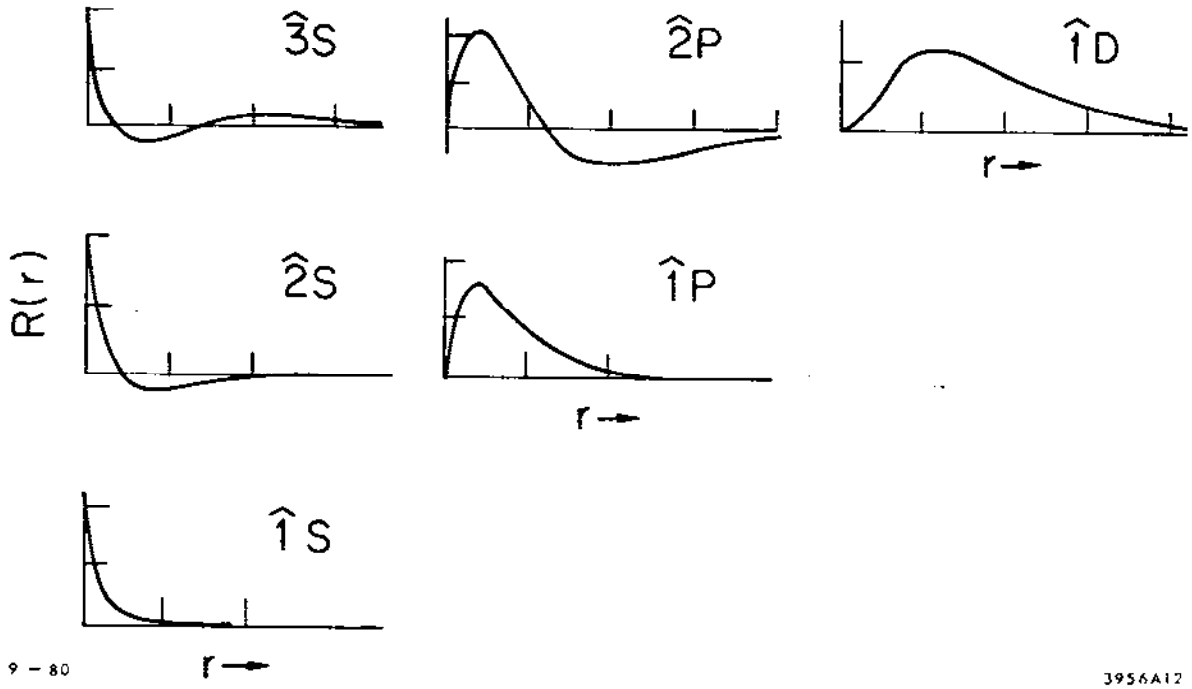

Fig. 3.3

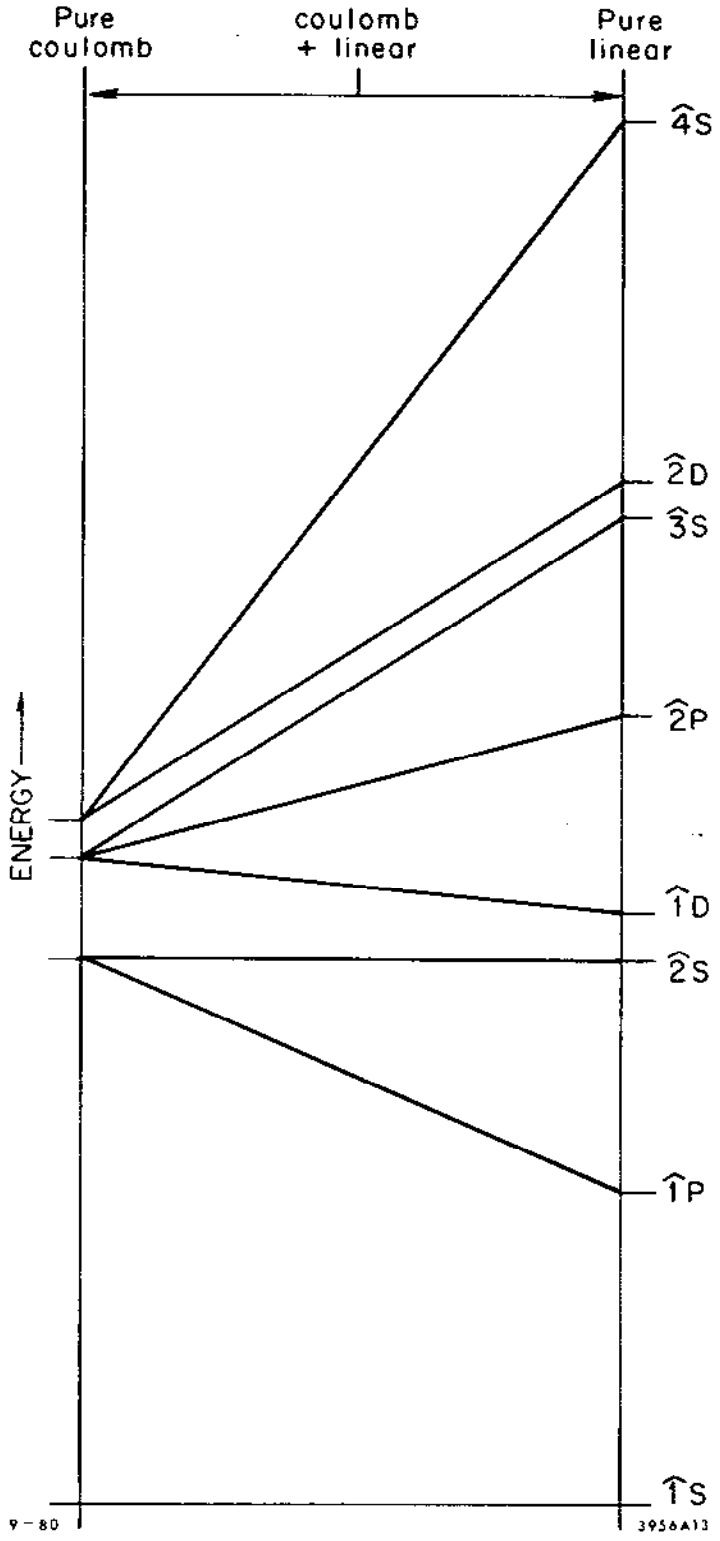
Pure coulomb
coulomb + linear
Pure linear
4̂S
2̂D
3̂S
2̂P
ENERGY
1̂D
2̂S
1̂P
1̂S
9-80
3956A13

Fig. 3.4

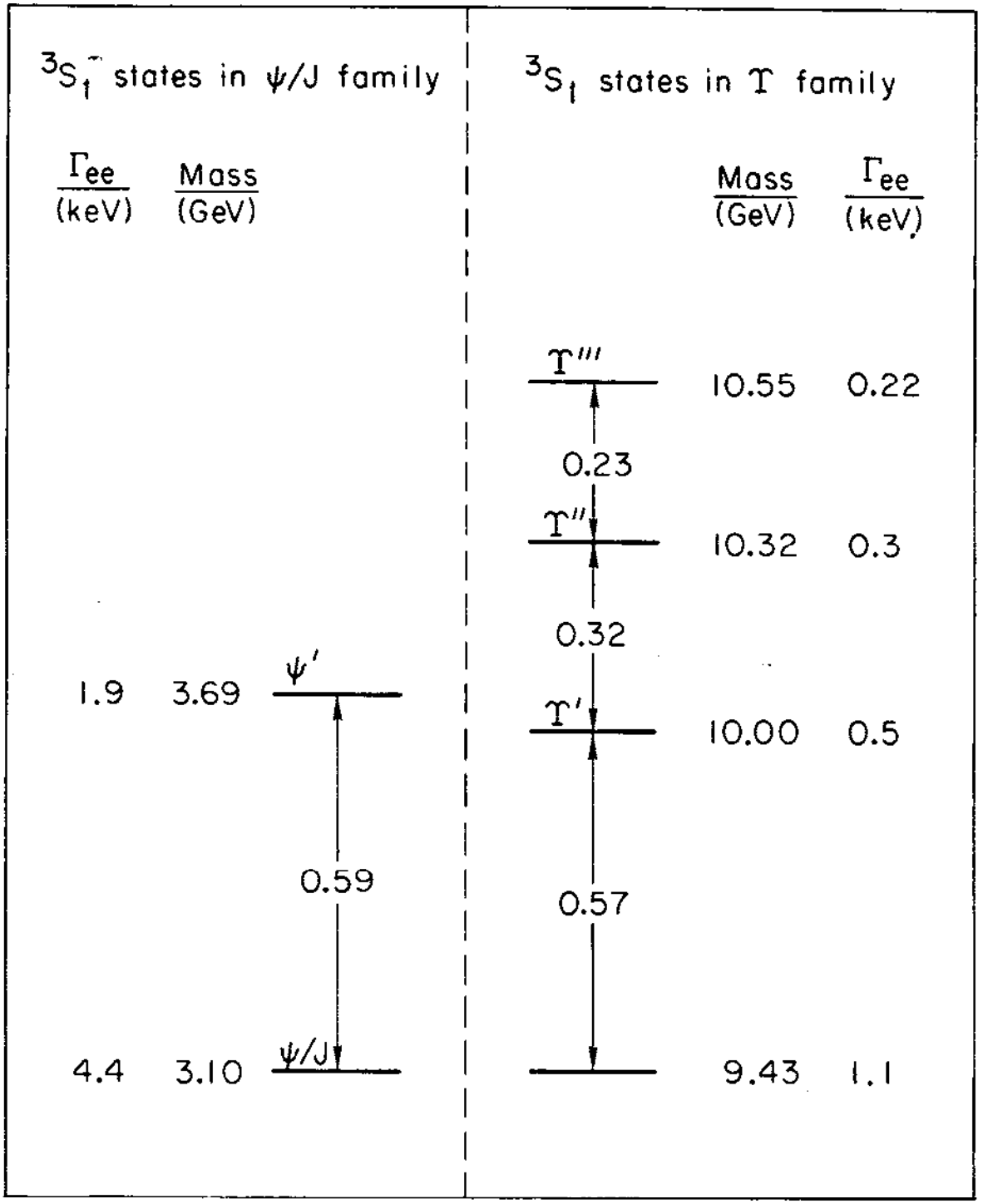
$^3S_1$ states in ψ/J family
$\frac{\Gamma_{ee}}{(keV)}$
$\frac{Mass}{(GeV)}$
1.9
3.69
ψ'
0.59
4.4
3.10
ψ/J
$^3S_1$ states in Υ family
$\frac{Mass}{(GeV)}$
$\frac{\Gamma_{ee}}{(keV)}$
Υ'''
10.55
0.22
0.23
Υ''
10.32
0.3
0.32
Υ'
10.00
0.5
0.57
9.43
1.1
9 - 80
3956A14

Fig. 3.5

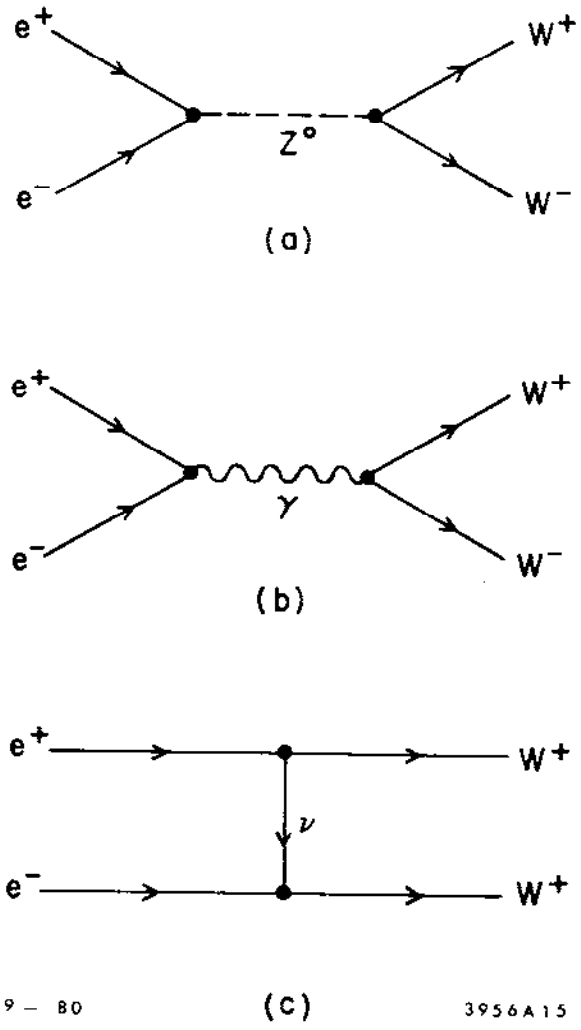

Fig. 4.1

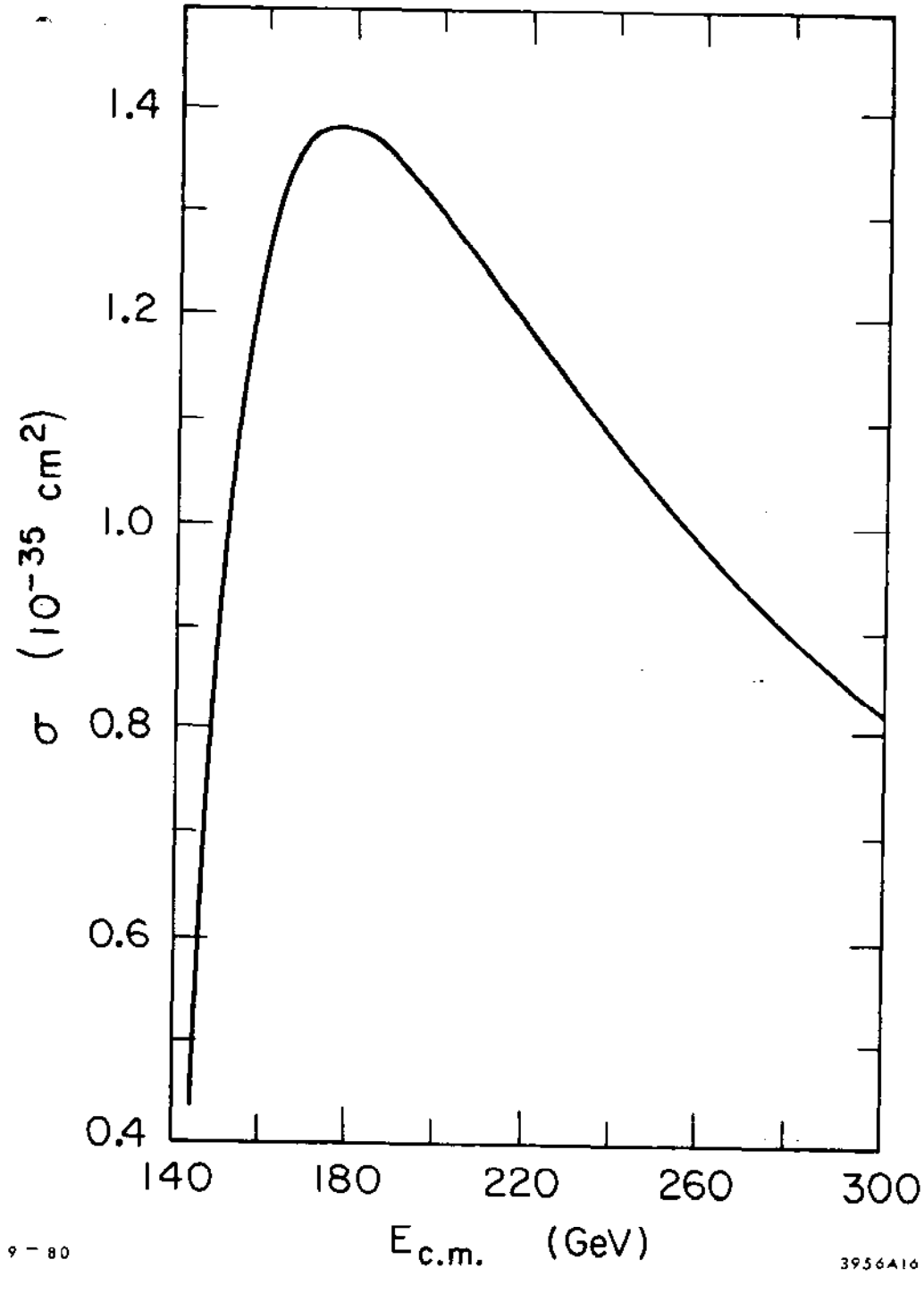
1.4
1.2
1.0
0.8
0.6
0.4
σ (10⁻³⁵ cm²)
140
180
220
260
300
E c.m. (GeV)
9 - 80
3956A16

Fig. 4.2

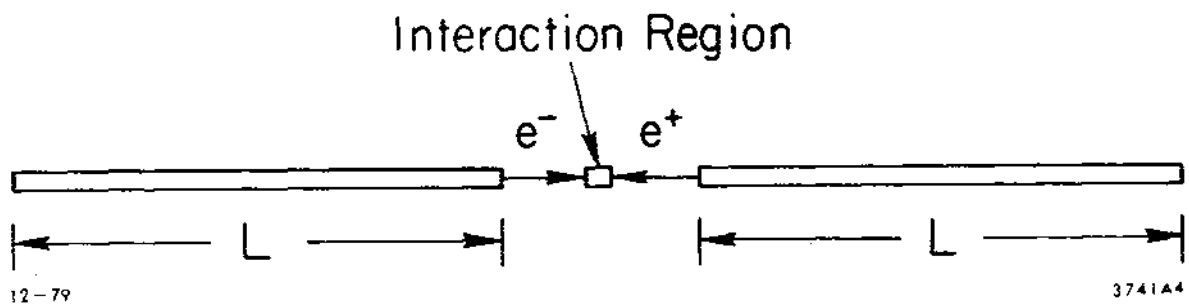

Fig. 4.3

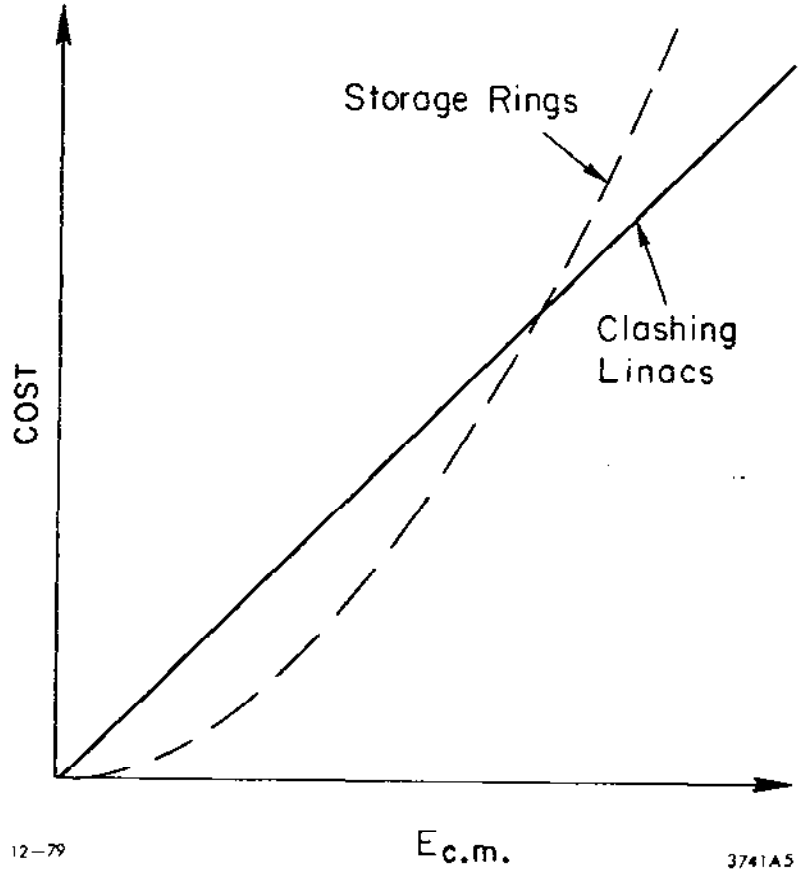

Fig. 4.4

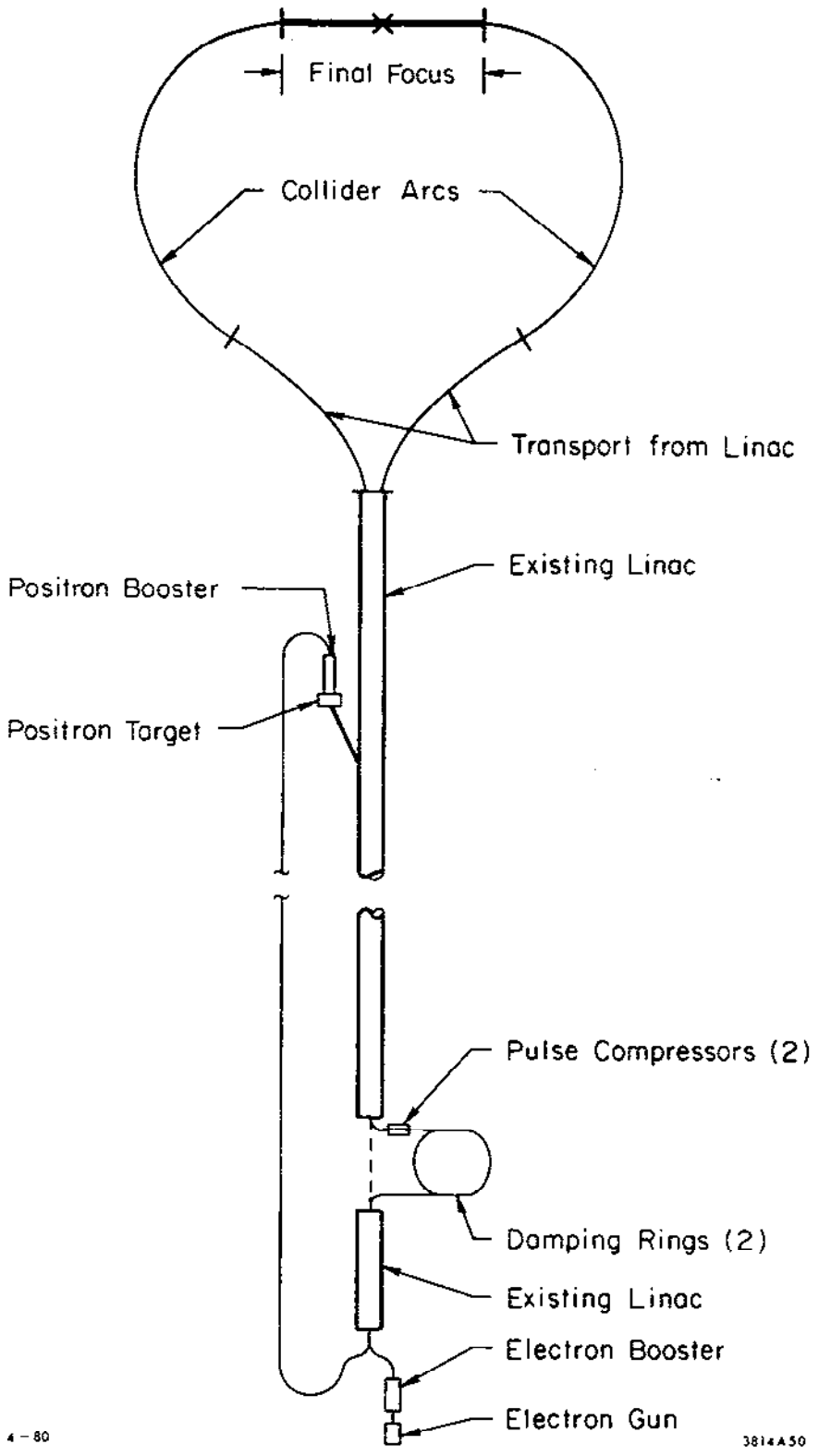
Final Focus
Collider Arcs
Transport from Linac
Existing Linac
Positron Booster
Positron Target
Pulse Compressors (2)
Damping Rings (2)
Existing Linac
Electron Booster
Electron Gun
4 – 80
3814A50

Fig. 4.5